Cavitation control using passive flow control techniques

Mahshid Zaresharif[1,2], Florent Ravelet[3], David J Kinahan[1,2,4,5] and Yan Delaure[1,2*]

[1]The Water Institute, School of Mechanical and Manufacturing Engineering, Dublin City University, Ireland

[2]Advanced Processing Technology Research Centre, School of Mechanical and Manufacturing Engineering, Dublin City University, Ireland

[3]Arts et Metiers Institute of Technology, CNAM, LIFSE, HESAM University, 75013 Paris, France

[4]I-Form - The SFI Centre for Advanced Manufacturing, Dublin City University, Ireland

[5]National Centre for Sensor Research, Dublin City University, Ireland

* Corresponding Author: Yan.Delaure@dcu.ie

Abstracts

Passive flow control techniques, and particularly vortex generators have been used successfully in a broad range of aero- and hydrodynamics applications to alter the characteristics of boundary layer separation. This study aims to review how such techniques can mitigate the extent and impact of cavitation in incompressible flows. This review focuses first on vortex generators to characterize key physical principles. It then considers the complete range of passive flow control technologies; including surface conditioning and roughness, geometry modification, grooves, discharge, injection, obstacles, vortex generators, and bubble generators. The passive flow control techniques reviewed typically delay and suppress boundary layer separation by decreasing the pressure gradient at the separation point. The literature also identifies stream-wise vortices that result in the transfer of momentum from the free stream to near-wall low energy flow regions. The

area of interest concerns hydraulic machinery, whose performance and life span are particularly susceptible to cavitation. The impact on performance includes a reduction in efficiency, and fluctuations in discharge pressure and flow, while cavitation can greatly increase wear of bearings, wearing rings, seals and impeller surfaces due to excessive vibration and surface erosion. In that context, few studies have also shown the positive effects that passive controls can have on the hydraulic performance of centrifugal pumps, such as total head and efficiency. It is conceivable that a new generation of design in hydraulic systems may be possible if simple design features can be conceived to maximize power transfer and minimize losses and cavitation. There are still however significant research gaps in understanding a range of impact factors such as manufacturing processes, lifetime, durability, and essentially how a static design can be optimized to deliver improved performance over a realistic range of operating conditions.

Keywords

Passive flow control, Cavitation control, Vortex generator, Boundary layer separation

Nomenclature

ACL	Anti-cavitation Lip	Ra	roughness
c	Hydrofoil chord	Re	Reynolds number
CGs	Cavitating bubble Generators	Re_θ	Reynolds number based on momentum thickness
CCGs	Cylindrical Cavitating bubble Generators	R-T	Rayleigh–Taylor
C_D	Drag coefficient	S	Hydrofoil Span
C_{pmin}	Minimum pressure coefficient	TLV	tip-leakage vortex
GEMS	gas entrapment by micro-textured surfaces	U_∞	Free-stream stream-wise velocity
h	Device height	VG	Vortex generator
h/ δ	Device height to boundary layer thickness ratio	X_{VG}	Distance between the leading edge and vortex generators
K-H	Kelvin-Helmholtz	z	distance between two Doublet Wheeler or Wishbone Wheeler vortex generators
l	Device chord length	α	Angle of attack
L	Distance between two counter-rotating vortex generators' ends	β	Device angle of incidence
LSB	laminar separation bubble	δ	Boundary layer thickness
m	Vortex Generators spacing in the span-wise direction between two pair of counter-rotating vortex generators	Δh	height of the cavity
mVG	Micro Vortex Generator	Δs	distance between the leading edge roughness and the re-entrant jets
n	Gap ratio of between two counter-rotating vanes	ΔX_{VG}	Distance between the vortex generators trailing edge and

			baseline separation line
NPSH	Net Positive Suction Head	λ	Distance between two co-rotating vortex generators
OHG	overhanging grooves	σ	Cavitation number
PIV	Particle image velocimetry		

Introduction

Cavitation is defined as the appearance of vapor cavities due to phase change in a liquid medium [1]. Hydraulic machinery in industries have been experiencing many challenges which are associated with the cavitation phenomenon include noise [2], vibration [3], material damage [4], and reduced efficiency/performance [5].

Since the initial investigation of Reynolds[6], there have been many studies that have attempted to improve our understanding of the nature of the phenomenon; focusing, amongst others, on processes involved in the formation of cavitation vapor, the dynamics of bubble detachment, the behavior of boundary layers, and more recently, on how the strength, extent, dynamics, and impact of cavitation may be controlled or mitigated. The two essential prerequisite conditions needed for cavitation to develop are the presence of favorable bubble inception sites and the opportunity for the liquid pressure to fall below the saturation pressure. Dissolved gas in the liquid medium can also play a role in the activation of nucleation sites. These prerequisites commonly occur in hydraulic machinery. Sudden pressure drops over impellers and blades occur as energy in the flow is transferred to kinetic energy in the volute and around impeller blades [7].

Initially, the bubbles in the oncoming stream on a hydrofoil or generally a surface were assumed to be micron-sized nuclei in the liquid and they would move along the streamline close to the solid

surface. Observable bubbles of 1 mm or larger were deemed to initiate cavitation. Nuclei present in incident-free streams are a primary source of these bubbles. Nuclei passing close to the front stagnation point will experience large fluid accelerations and pressure gradients since the streamlines encountering the low-pressure region are close to the surface. The initial growth phase in all cases was characterized by a spherical cap. Bubbles are separated from walls by thin layers of liquid of a thickness equal to the boundary layer. Once the bubble enters an area of adverse pressure gradient, it begins to be pushed inward, resulting in a wedge-shaped profile. Thus, the bubble collapse begins on the exterior frontal surface, often resulting in the bubble breaking into forward and aft bubbles. This phase is called bubble travelling cavitation [8-10].

As the bubble grows, it develops substantial span-wise vorticity as it interacts with the boundary layer. As a result, the cavitating vorticity within a bubble is concentrated as the collapse proceeds, transforming it into one (or several, or even more) cavitating vortex with a spanwise axis. When the vortex bubbles collapse, they reappear as a cloud of small bubbles. There is an occasional occurrence where bubbles pass the point where the laminar separation occurs and subsequently develop locally attached cavitation streaks at the lateral or span-wise extremities of the bubble.

This trailing edge of attached cavitation, which is attached to the solid surface, eventually extends out behind the main bubble. Consequently, the main bubble collapses first, leaving the tails to persist for a fraction longer. At this point an attached cavity is generated which can evolve to other type of cavitation such as cloud cavitation or supercavitation (Table 2) [9, 11].

Once formed, cavities will eventually collapse or release clouds that will collapse resulting in a shock wave [12], and a focus of energy toward walls which typically lead to cavitation erosion and noise. Over the past four decades, significant research effort has been dedicated to investigate how

cavitation may be controlled. This work has tended to focus on extruded profiles from hydrofoils, propellers, pumps, and turbine blades.

Stabilizing cavity resonance or reducing volume of wall and near wall cavities are two solutions to control, reduce or eliminate cavitation. The presence of nuclei and micro-bubbles within liquids and at solid surfaces, surface characteristics, and Reynolds number are some factors that affect cavitation [13-17]. Adjustment or modification of one or all of these parameters can allow for effective cavitation control. However, the most important parameters which impact cavitation have been linked to the control of boundary layer separation [1, 18, 19].

The laminar separation can be generated downstream of an adverse pressure gradient and make a low pressure region. The separated layer can then shelter the oncoming flow and generate an attached separation cavity with low pressure at the core. It was found that suppressing or eliminating this separation can effectively delay or suppress the formation of an attached cavity [20]. The higher momentum of the turbulent flow improves its ability to resist adverse pressure gradient over convex surfaces and hence limit the incidence of separation [1, 21]. Compared to turbulent boundary conditions, a laminar boundary flow is more likely to separate, resulting in a higher drag penalty. The control of boundary layer separation achieved by triggering an early transition to a turbulent boundary layer is therefore beneficial both in terms of its effect on drag and on cavitation. Other solutions have been considered and have shown varying degree of effectiveness.

Flow control techniques can be defined as tools to change the natural state of fluid flows and their transition into more controlled and desired flow conditions [22]. Flow control strategies are divided into two types: passive and active. Passive solutions include devices that do not rely on the controller or energy sources needed for active control [23]. Passive and active can be effective techniques to manipulate and change wall-bounded or free-shear flows. This change can be made

by delaying or inducing advanced transition, suppressing or boosting turbulence, and provoking or suppressing separation. These changes can increase lift, decrease drag, suppress flow-induced noise, and induce vortex mixing. Devices and structures that can manipulate the fluid dynamics of a system without an external power source include vortex generators (VGs), tailored surface roughness, injection and discharge channels, and surface obstacles, as well as grooves to redirect flow and change vortices regime.

Active controls include wall temperature increase, dynamic surface modification by deformation or movable parts, and injection or flow oscillation using blowing, suction, and synthetic jets [24].

This article aims to review studies focused on passive flow controls applied to cavitation. Amongst these, VGs are regarded as the most effective and simplest technique and have been used in many applications such as airfoils, wind turbine blades, swept wing, and heat exchangers [25]. Apart from their effectiveness on boundary layer separation, their simple design, low cost, and lower drag make them an effective tool in a broad range of applications [26]. Because of this, while other passive flow control technologies are also reviewed, a particular emphasis has been placed on VGs.

The application of passive flow control in compressible external aerodynamics has a significant history. Although there is a noticeable difference between compressible and incompressible flows in the behavior boundary layer separation [27], passive flow control studies in compressible flow can be a good guide and pattern for incompressible flow cavitation. It is possible to correlate the compressible flow boundary layer behavior to the incompressible flows using three assumptions: 1) the boundary layer is regarded as thermally insulating, 2) the viscosity changes with absolute temperature, and 3) the flow Prandtl number is unity [28]. The first section of the article reviews the literature on compressible single-phase flow studies. In the next section, different passive flow

129 controls are reviewed in the context of cavitation. The last section concludes on key results and
130 promising open research topics.

131 1. Passive flow control techniques in single-phase flow

132 In most aerodynamic applications, such as external flow over aircraft and ground vehicles, and
133 internal flows such as diffusers, boundary layer separation is typically an undesirable phenomenon.
134 Depending on the nature of the wake, separation induces periodic or random pressure variations.
135 Boundary layer separation also leads to weaker lift, increased drag, and energy losses. Finding
136 ways to control separation and, if possible, prevent it [29] is clearly desirable assuming the applied
137 control method has no impact on efficiency or energy consumption.

138 The idea of using passive flow control and vortex generation in hydro- or aerodynamic applications
139 is well established and has led to a broad range of studies. Since the late 1990s, several
140 investigations have been focused on the effectiveness of using different passive flow control
141 methods on boundary layer separation and aerodynamic performance [25]. According to the analysis
142 of drag coefficients for various Reynolds numbers on a smooth sphere compared to a rough sphere
143 or one with an obstacle, a drag crisis occurs at lower Reynolds numbers, also affecting boundary
144 layer separation (Figure 1) [30, 31].

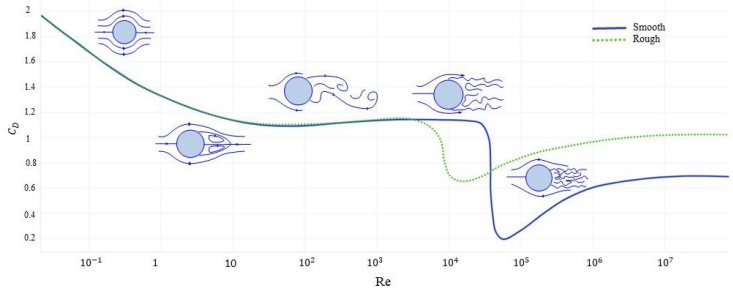

Figure 1 - Dependency of drag coefficient on Reynolds number for a smooth and rough sphere.

The results of these studies guide the implementation of passive control methods in cavitation studies. Vortex generators, distributed roughness, leading-edge slats [32, 33], flow vanes [34], leading-edge serrations [35], slotted airfoils [36] and suction and blowing techniques [24, 37, 38] have all been considered for application in external aerodynamics .

There is ample evidence that increased surface roughness can be harnessed to induce vortex shedding, insert energy into the boundary layer, and trigger an early transition to turbulence. This has been shown to delay boundary layer separation and increase the extent of the attached flow region [39, 40]. Effects reported include lift recovery and noise reduction [41, 42]. Surface roughness is also effective in postponing stall phenomena and improving an airfoil's aerodynamic performance [40].

VGs were initially introduced as small aerodynamic devices attached to a part of an aerodynamic vehicle. They are able to generate a small vortex downstream. VGs can have a similar effect transferring momentum from the free stream to the near wall region. They can provide one of the most practical means to control flow separation over airfoils because of their small size [43]. Benefits include increased lift, delayed stall and drag reduction. Most of the published research in this field concentrates on finding a design that optimizes the vortex generators' height, geometry and

location upstream of the separation line. The most important parameters are the geometry, the height h, the height to pitch ratio, h/δ, the array layout, ΔX_{VG}, l/h and β. Different VG designs and their important parameters are shown in Figure 2.

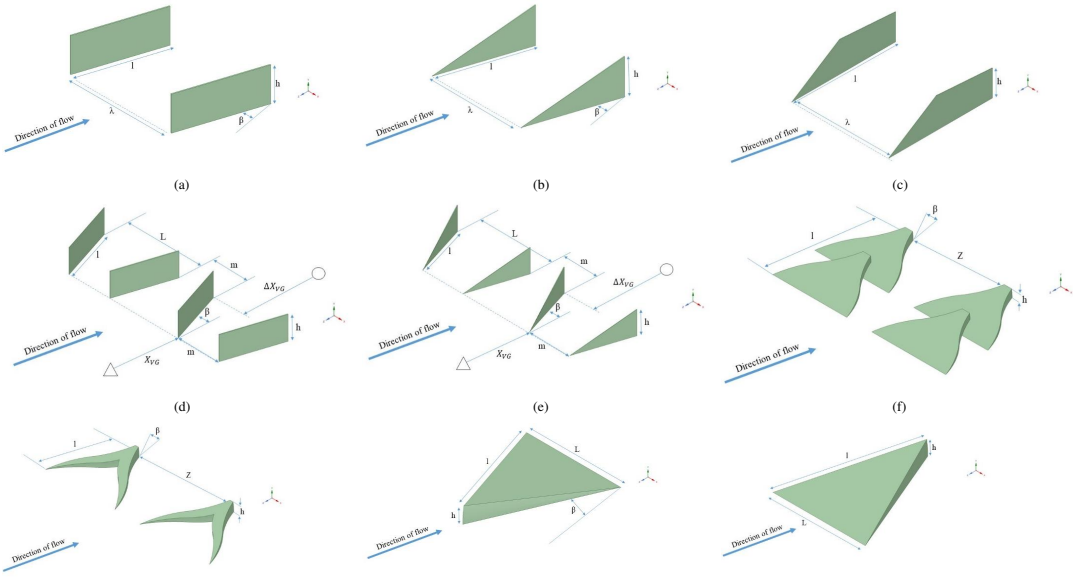

Figure 2 - Schematic of vortex generators with key design parameters, (a)Co-rotating Rectangular Vortex generators, (b) Co-rotating Dalta-shaped Vortex Generators, (c) Co-rotating Gothing Vortex Generators, (d) Counter-rotating Rectangular Vortex Generators (m=0 joined vanes and m>0 spaced vanes), (e) Counter-rotating Dalta-shaped Vortex Generators (m=0 joined vanes and m>0 spaced vanes), (f) Doublet Wheeler Vortex Generators, (g) Wishbone Wheeler Vortex Generators, (h) Forward Wedge (Micro-ramp) Vortex Generators, (i) Backward Wedge (Micro-ramp) Vortex Generators, which h=Device height , l= Device chord length, m=Vortex Generators spacing in the span-wise direction between two pair of counter-rotating vortex generators, β=Device angle of incidence, X_{VG}= Distance between the leading edge and vortex generators, ΔX_{VG}=Distance between the vortex generators trailing edge and baseline separation line, L=

Distance between two counter-rotating vortex generators' ends, λ= Distance between two co-rotating vortex generators and Z= distance between two Doublet Wheeler or Wishbone Wheeler vortex generators

166

Inducing stream-wise instabilities and vortices is one of primary ideas for suppressing the boundary layer separation. In the 1970s, Kuethe[44] observed a type of centrifugal instability called Taylor–Goertler that can lead to the formation of arrays of stream-wise vortices over a concave surface. They tested wave-type VGs and with h/δ in the range 0.27 to 0.42. They observed that VGs caused stream-wise vortices in the boundary layer because of a Taylor–Goertler instability. VGs were used to suppress the Kármán vortex stream and to reduce acoustic disturbances in the wake area. They could also confine the velocity deficit region in the wake resulting in improved performance.

Rao and Kariya[45] investigated so-called submerged VG where the VG height was kept smaller than the boundary layer ($h/\delta \leq 0.625$). A comparison with conventional VGs ($h/\delta \sim 1$) showed that a much lower parasitic drag and better performance in boundary layer separation could be achieved by confining the VG in the boundary layer. Since this seminal work, research has focused on these so-called submerged VGs [45-49] which have also been called micro-VGs [50-53], sub-boundary-layer VGs [54, 55], and micro-vanes [56]. It has been shown in particular that VGs with $0.1 \leq h/\delta \leq 0.5$ could provide sufficient momentum transfer towards the wall and over extended downstream region. With a smaller footprint, submerged VGs have also proven to be more versatile for a wider range of applications.

Research on micro-vortex generators (mVGs) has targeted two main research questions; how effective are mVGs at delaying boundary layer separation and what type of vortical flow is generated downstream. A summary is presented in Table 1 where studies are classified based on the VGs characteristic parameters such as geometry and location for effective flow control [26].

Lin et al. conducted important experimental studies on the mVGs effectiveness on boundary layer using a 2D backward-facing curved ramp at low speed at NASA Langley Research Center [46, 47, 49,

[50]. They tested numerous mVGs and other passive flow control methods. Their performance measured in terms of the relative reduction in the extent of the separation region is shown in Figure 3, with the VG geometries defined in (a, d, f and g). The most effective methods, such as mVGs and large longitudinal surface grooves, were shown to generate stream-wise vortices. mVGs (counter-rotating and co-rotating vane-type VGs with h/δ~0.2 and h/δ~0.8) and Wheeler VGs (wishbone and doublet) were found to have almost the same effects on separation delay. Other methods such as span-wise cylinders and transverse grooves generated higher form of drag and proved less effective [47, 49, 50].

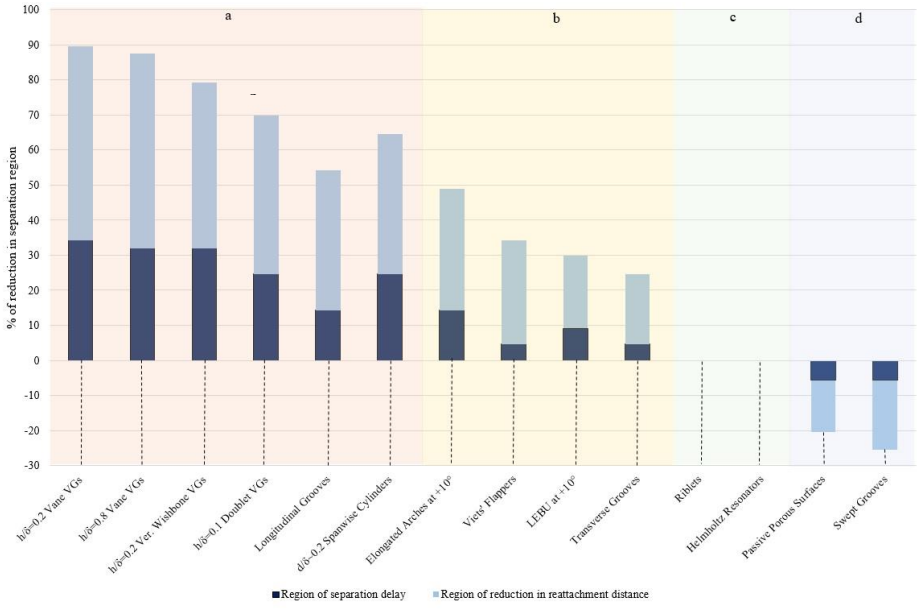

Figure 3 - Effectiveness of micro-vortex generators and other passive flow control methods on the extent of the separation region. (a) A group of devices that generates stream-wise vortices and proved most effective at suppressing boundary layer separation; the submerged vortex generators being the most effective, and longitudinal producing the lowest effect (b) Devices that generate transverse vortices, which are still effective; span-wise cylinders and transverse grooves having the highest and lowest effect

respectively (c) The drag reducing riblets and Helmholtz resonators have no actual effect on boundary layer separation, (d) passive porous surfaces and swept grooves have the potential to enhance boundary layer separation [50].

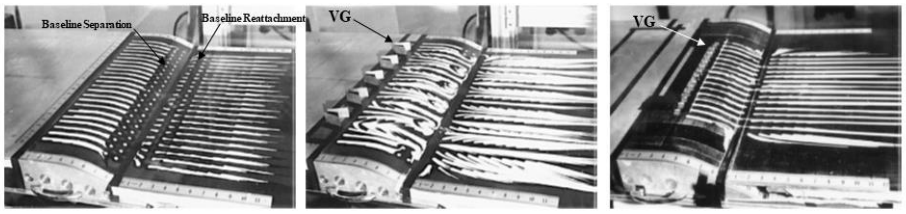

a b c

Figure 4 - Oil-flow visualizations of the effect of vortex generators for flows over a backward-facing ramp for the (a) baseline case without vortex generators which produces an obvious two-dimensional separated flow (b) Counter-rotating conventional vane-type vortex generators (h/δ~0.8) placed 5δ upstream of a baseline separation which could produce an attached flow downstream of the ramp albeit with strong three-dimensional features including a visible recirculation zone downstream of the separation baseline , (c) Vane-type counter-rotating vortex generators (h/δ~0.2) placed at 2δ upstream of baseline separation which could suppress the boundary layer sufficiently with lower three-dimensional variations in the span-wise pressure at the shoulder region of the ramp [50]. From Control of turbulent boundary-layer separation using micro-vortex generators, J. Lin, American Institute of Aeronautics and Astronautics, Inc, In the public domain.

In Figure 4, Visualization of oil flow separation downstream of the baseline surface (without VGs) (Figure 4 (a)) were compared with conventional counter-rotating VGs with flow at 6 h and 10 h upstream of baseline separation (Figure 4 (b) and (c)). The results of the study found that vortices generated by conventional VGs are stronger than needed and yet are not suppressing separation, while the mVGs achieved close to a 90% reduction in separation and did not generate pockets of recirculating flow. Measurements of surface pressure along the stream-wise direction and at three span-wise locations shown in Figure 5, clarified the role of mVGs in eliminating separation. Most notable is the lower three-dimensional variability in pressure distribution along the span-wise direction on the shoulder region of the ramp.

Lin et al. [49] examined the impact of further reduction in h/δ from 0.2 to 0.1 and observed a deterioration in the mVG effect on separation. These results confirmed that mVGs can be more effective in controlling flow separation than larger VG but care must be taken in determining an effective height to boundary layer thickness ratio to avoid.

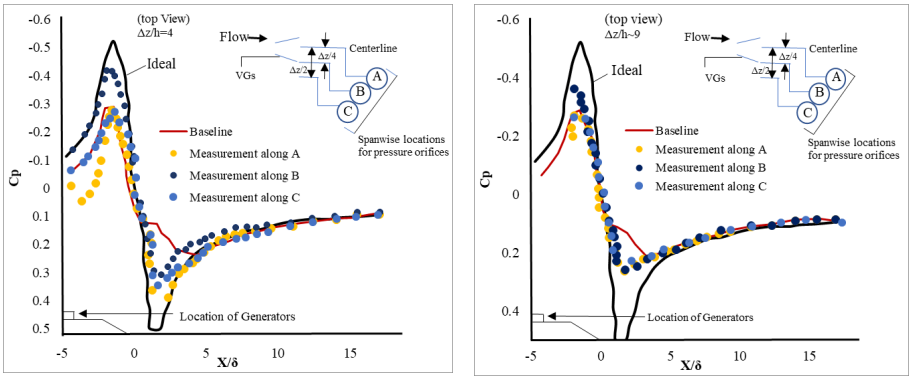

a b

Figure 5 - Span-wise variations in the stream-wise pressure distribution with (a) conventional vane-type counter-rotating vortex generators (h/δ~0.8) placed at 5δ upstream of baseline separation, which shows noticeable differences between the three span-wise positions, (b) Counter-rotating vane-type micro-vortex generators placed 2 δ upstream of the baseline separation, which show a lower span-wise pressure variation compared to conventional vortex generators[50]. From Control of turbulent boundary-layer separation using micro-vortex generators, J. Lin, American Institute of Aeronautics and Astronautics, Inc, In the public domain.

Ashill et al. [55] performed a comparative study on wedge type and counter-rotating mVGs located $52h$ upstream of the baseline separation line. The counter-rotating mVGs (Figure 2 (e)) with a $1h$ span-wise gap proved most effective at suppressing boundary layer separation.

Gorton et al. [51] studied the effects of mVG profile changes (Figure 6) in suppressing separation from a backward-facing ramp with co-rotating Gothing VGs (Figure 2 (c)). The study relied on oil-flow visualization illustrated in Figure 7. Figure 7 (a) shows two large spiral nodes and a central reverse flow at the ramp in the baseline case. The mVGs proposed by Gorton et al. [51] with $h/\delta \sim 0.2$ is shown in Figure 7 (b) to alter the direction of near-wall flow sufficiently to suppress separation.

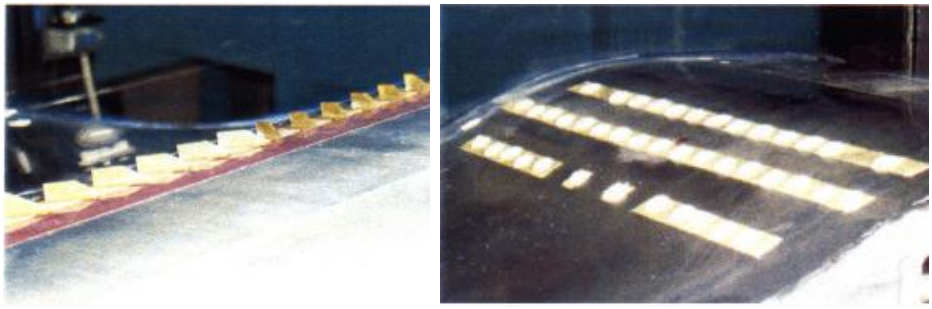

a b

Figure 6 - (a) Co-rotating Gothing micro-vortex generators configured at an angle of 23 degrees to the onset flow were created by Gorton et al. [51], which resulted in significant pressure gradient reduction, and (b) Installation of micro-bump arrays on the ramp with a maximum height of 10% of the boundary layer thickness [51]. From Flow control device evaluation for an internal flow with an adverse pressure gradient, S. Gorton, L. Jenkins, and S. Anders, American Institute of Aeronautics and Astronautics, Inc, In the public domain.

Ashill et al. [54, 55] also studied the flow characteristics of mVGs at the UK Defense Evaluation Research Agency Boundary Layer Tunnel. They performed tests for a range of mVGs with $h/\delta \sim 0.5$, including the single vane, counter-rotating vane-type, forwards, and backward wedges shown in Figure 2. The generated vortex strength was estimated from flow field measurements

using a laser doppler anemometer up to $15h$ downstream of the mVGs [55] and up to $50h$ downstream of the mVGs [54] . They proposed a correlation for the non-dimensional circulation and used the concept of a mVG sufficient height [55]. The correlation provides a prediction of the VG vortex strength downstream and is applicable for a wide range of Reynolds numbers. No relation is provided, however, between the sufficient height and a physical dimension of the mVGs. The study found that forwards-wedges and the joint-vane mVG create counter-rotating vortices sharing a mutual interface [55]. Measurements indicated that this led to reduced vortex strength. The vortices generated by backward wedge mVGs were found to be always closer to the wall impacting on wall shear.

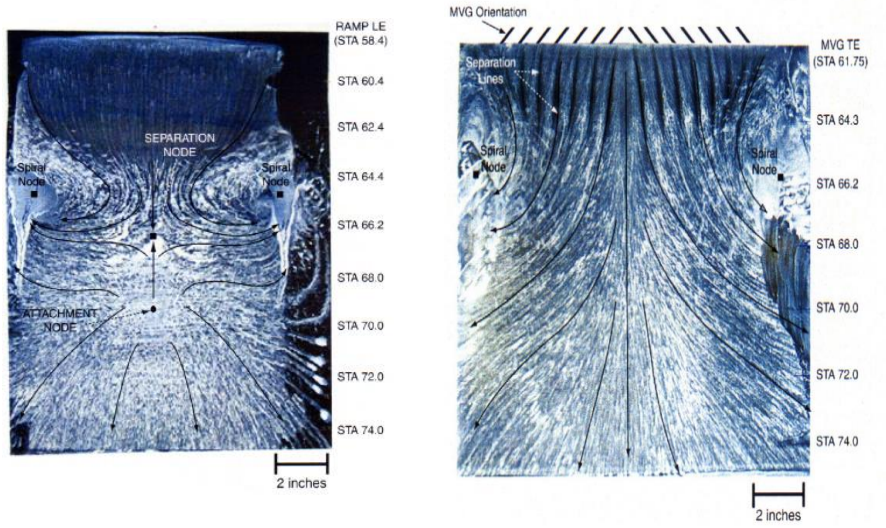

a b

Figure 7 - (a) Oil flow visualization of baseline case for flow over a backward-facing ramp with vortex generators and at an onset velocity of 42.7 m/s. The image provides evidence of large spiral nodes and a central reverse flow. (b) Oil flow visualization of the effect of vane-type co-rotating Gothing micro-vortex generators with h/δ ~0.2 in comparison with the

baseline case using which direction change of near wall flow and suppressing reversing flow is shown [51]. From Flow control device evaluation for an internal flow with an adverse pressure gradient, S. Gorton, L. Jenkins, and S. Anders, American Institute of Aeronautics and Astronautics, Inc, In the public domain.

Counter-rotating vane mVGs were shown to double the vortex strength when tested up to 50 h downstream of the mVGs. The joined-vane and the forwards-wedge mVGs produced stronger vortex decay than the two 1 and 2 h spaced counter-rotating vanes mVGs at a downstream distance of up to 15 h . In terms of adverse pressure gradient, spaced vanes proved to be more efficient than joined vanes. In comparison to counter-rotating vanes, forward-wedge mVGs reduced drag by 60%. According to the analysis of counter-rotating vanes, increasing the gap ratio can help decrease the generated drag of devices.

In other studies, Yao et al. [57] and Allan et al. [58] conducted an experimental and numerical analysis of single vane-type mVGs on a flat plate. A flow field measurement system was developed to characterize embedded stream-wise vortices downstream of mVGs. Their system consisted of a 3D stereo imaging and particle image velocimetry (PIV) system covered downstream vane-type mVGs. CFD and experimental results both demonstrated that downstream of mVGs, vortices decay substantially regardless of the device incidence angle.

The effectiveness of wedge-shaped and counter-rotating vane mVGs interaction with shocks and boundary layer at Mach numbers of 1.5 and 1.3. was also investigated by Holden and Babinsky[59]. They observed that both types of mVGs affected the separation bubble under shock and the vortex intensity. Although the vane type mVGs were shown to have a stronger effect because of the higher vortex strength closer to the surface, both types of mVGs can create a wave pattern consisting of shocks, re-expansions, and shocks. Wave drag and pressure losses increase due to this pattern. It

was also observed that wedge-shaped mVGs generated vortices that lifted off the surface more quickly.

Babinsky et al. [60] and Ghosh et al. [61] conducted experimental and CFD analyses of forward wedge type mVG. The formation and evolution of multiple pairs of counter-rotating stream-wise vortices were observed downstream of the mVGs as shown in Figure 8. A low-momentum region forms in the wake of the wedge along the centerline between consecutive mVGs. The magnitude of momentum deficit was found to be proportional to the size of mVGs and inversely proportional to the drag induced by wedge-type while the two counter-rotating vortices act to transfer high momentum from the boundary layer peripheral region to the surface. Despite the strongest effects and greatest drag caused by the largest mVGs, the smallest mVGs ($h/\delta = 0.3$) had similar effects on separation with lower induced drag . The results also indicated that mVGs should be located closer to the adverse pressure gradients region than traditional VGs.

Dong et al. [62] proposed a new slotted ramp-type mVGs and numerically investigated their effect on the flow separation in supersonic flow. A more complicated wake structure was observed, including two confluent counter-rotating stream-wise vortices and an increase in number of stream-wise vortices. The interaction of these vortices with the primary counter-rotating vortex pair could increase the lifetime of vortices and boost the vortex intensity. These slotted mVGs also decrease the generated drag compared to standard micro-ramps and improve the separation control performance.

Sun et al. [63] developed a conceptual description of the evolution of the vortical structures in the wake of the micro-ramps in supersonic flows as illustrated in Figure 9. Based on Li and Liu[64] and Sun et al. [65], velocity shear and, consequently, pressure gradients downstream of micro-ramps induce swirling vortices in an arc or ring shape. The mechanism of vortex generation can be linked

to Kelvin-Helmholtz (K-H) instabilities. The model of Sun et al. [63] depicts the dynamics of vortices in stages of K-H evolution. Initially, the stream-wise vortices generated as focused filaments which quickly lose their stability and change into arch-shape K-H vortices. The wavelength of the instability starts to increase due to shear velocity and vortex pairing increase. As the legs of the arch-shaped K-H vortices grow and merge with neighboring vortices, vortex rings are eventually formed. As a result of stream-wise vortices, downward motion is induced at this stage. Turbulent distortion eventually causes the ring vortices to break down.

Sun et al. [66, 67] also conducted a numerical modelling to analyze the wake of micro-ramp VGs under hypersonic conditions. They observed a type of arch-type vortices that grow moving downstream and breaking the primary vortices. They found that these mVGs can generate span-wise structures caused by the impinging of the arc-like vortices. Their result showed that drag and heat flux was reduced after applying mVGs to change the cortical structure pattern.

Other applications of passive control in compressible flows not in the scope of this article are reviewed in detail by Akhter and Omar[68] and Genç et al. [25].

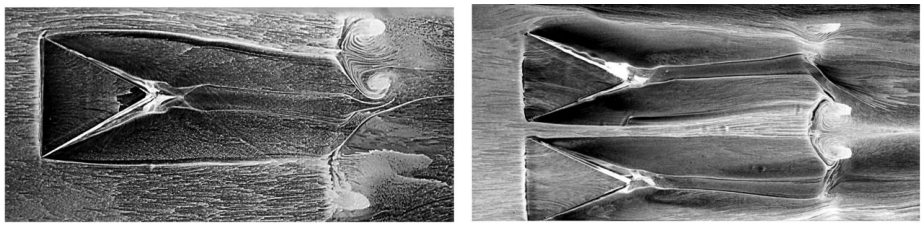

a *b*

Figure 8 - A surface oil-flow visualization for flow over micro-ramp developed by Babinsky [60] et al. Implementation of micro-ramps generate a region of attached flow in its immediate downstream centerline and break down the overall separation region into small individual separation areas. The generation of stream-wise vortex pairs is shown to develop in both individuals and array of micro-

ramps. From Micro-ramp Control of Supersonic Oblique Shock-Wave/Boundary-Layer Interactions, H. Babinsky, Y. Li, and C. W. P. Ford [60]; reprinted by permission of the American Institute of Aeronautics and Astronautics, Inc.

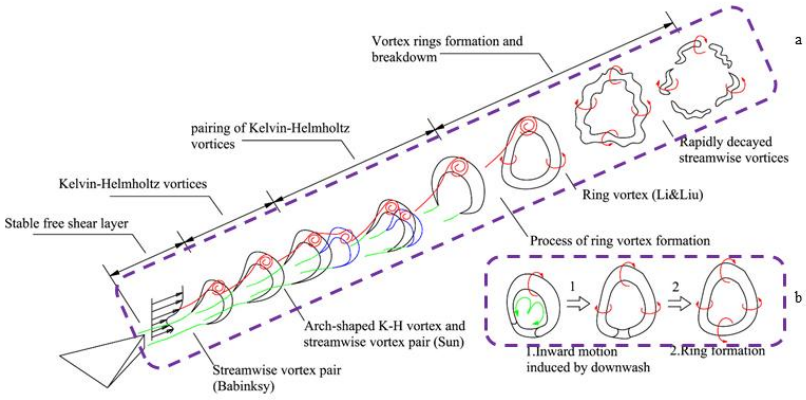

Figure 9 - Conceptual model of vortical structures created by micro-ramps [63]. (a) The stream-wise vortex pairs are initially generated immediately downstream of the micro-ramp. As a result of the instability of the curved free shear layer around the wake, these vortexes developed into arc-shaped Kelvin-Helmholtz vortices. Kelvin-Helmholtz vortices pair with each other, and mean shear velocity increases which cause the instability wavelength to increase. Kelvin-Helmholtz vortex rings are formed by the leg portions of arch-shaped vortices extending to the bottom side of the turbulent wake. These vortex rings break down downstream as a result of turbulent distortion. (b) process of vortex ring formation. Republished with permission of *American Institute of Physics*, from *Decay of the supersonic turbulent wakes from micro-ramps*, *Z. Sun, F. Schrijer, F. Scarano, and B. Oudheusden*, *Physics of Fluids 26, 025115 (2014)*; permission conveyed through Copyright Clearance Center, Inc.

314 *Table 1- Summary of research for effectiveness of micro-vortex generators on boundary layer separation* [26]

Investigator (s) *(Year pub.)*	*Test condition*	U_∞ [i] $[m/s]$	Re (Re_θ [ii])	Mach	δ [iii] $[mm]$	*VG type*	*VG parameters*					*Comments*
							h/δ [iv]	l/h[v]	m/h[vi]	β[vii] $[° deg]$	$\Delta X_{VG}/h$[viii]	
Lin et al. [46] (1990)	Wind–tunnel test low speeds Backward–facing ramp	40.2	(9×10^3)	NA	32.5	Doublets	0.1	~13	8	±25	20	Most effective Doublet VGs in separation control: h/δ~0.1.
Lin et al. [47 49] (1990-1991)	Wind-tunnel test Backward–facing ramp	40.2	(9×10^3)	NA	32.5	Wishbones	0.2	~3	4	±23	10	Most effective Reverse Wishbone VGs in separation control: h/δ=0.2.
Lin [50](1999)	Wind-tunnel test Backward–facing ramp	40.2	(9×10^3)	NA	32.5	Counter-rotating rectangular vanes	0.2	4	9	±25	10	Most effective counter-rotating vanes VGs: h/δ~2. ↑ Embedded stream-wise vortices
Ashill et al. [55] (2001)	Wind–tunnel test Bump	20	19×10^6 (35×10^3)	0.68	33	Counter–rotating delta vanes	0.3	~10	12	±14	52	Counter-rotating vanes VG with 1 h spacing have more potential for control boundary layer separation.
						Forward wedges	0.3	10	12	±14	52	
Ashill et al. [54 55] (2001-2002)	Wind–tunnel test and CFD	$10 - 40$	NA	NA	60	Counter-rotating vanes	0.5	~10	NA	±14	15	Vortex strength has been correlated with

	Flat plate					Forward wedge	0.5	10	NA	±14		device Reynolds number. ↓Interference between mutual vortices caused by the spacing between counter-rotating VGs. ↓Vortices and drag.
						Backward wedge	0.5	10	NA	±14	50	
						Single vane	0.5	10	NA	10, 20, 30,45		
Gorton et al. [51] (2002)	Wind–tunnel test Backward–facing ramp	42.7	NA	NA	22.1	Co–rotating trapezoid vanes	0.2	4	4	23	12&9	Most rotating Co-rotating trapezoid vanes VGs: Low profile VGs induced a pair of juncture vortices.
Yao et al. [57] (2002)	Wind–tunnel test Flat plate	34	NA	NA	35	Single rectangular vane	0.2	0.7	NA	10, 16,	100	↑Embedded stream-wise vortex.
Allan et al. [58] (2002)	CFD Flat plate	34	7.2×10^6	NA	45	Single trapezoid vane	0.2	7	NA	10,23	15,27, 102	CFD underestimated the peak vorticity near the VG.
Holden and Babinsky[59] (2004)	Wind–tunnel test Backward–facing ramp	NA	28×10^6 (26×10^3	1.3 & 1.5	1.5	Wedge–type	1	10	12	NA	33	Both type of mVGs effects on the separation bubble under shock and vortex intensity. Vane type mVGs have stronger effect because of stronger vortices close to the surface Wave patterns that result from either mVG contain shocks, re-expansions, and shocks.
						Vane–type counter-rotating	0.83	10	12		40	

												The pressure losses result in an increase in wave drag.
Ghosh et al. [61]; Babinsky et al. [60] (2009-2010)	Wind-tunnel test-blowdown supersonic tunnel	NA	40×10^6	2.5	6.67	Micro-ramps	0.3 − 0.9	7.2	7.5	±24	13.3 − 16.7	↑The number of counter-rotating stream-wise vortices The largest mVGs have the strongest effect, while it also has the greatest drag. mVGs should be located near the adverse pressure gradients than traditional VGs Device height is likely to affect optimum location
Dong et al. [62] (2017)	Wind-tunnel test-Continuous supersonic tunnel	NA	(3.137×10^4)	1.5	1.125	Slotted Ramp-type	1.78	7.2	NA	±24	21.1	↑Complex wake structure comprised of a confluent counter-rotating stream-wise vortex pair and additional stream-wise vortices ↑ Life time, and strengthen the vortex intensity of primary vortex pairs ↓Generated drag Improving the separation control performance
						Ramp-type	1.78	7.2		±24	21.1	

Sun et al. [66, 67] (2019-2020)	Wind-tunnel test	NA	2.3 $\times 10^3$	5.0	5.17	Micro-ramps	0.25, 0.58, 0.77	7.2	NA	± 24	16.6	↓ Drag and heat flux Changing the cortical structures pattern generating span-wise structures which are caused by the Impinging of the arc-like vortices

[i] Free-stream stream-wise velocity

[ii] Reynolds number based on momentum thickness

[iii] Boundary layer thickness

[iv] h=Device height

[v] l= Device chord length

[vi] m=Vortex generators spacing in the span-wise direction

[vii] β=Device angle of incidence

[viii] ΔX_{VG}=Distance between the vortex generators trailing edge and baseline separation line

As a conclusion of this section, the results show that mVGs can effectively control flow separation over airfoils. The most important effects relate to boundary layer separation. The generation of stream-wise vortices in the boundary layer, transfers momentum toward near the wall, delaying and suppressing boundary layer separation, increasing lift and decreasing drag and pressure recovery downstream of VGs. The mVGs are quite efficient in suppressing shock-induced separation in supersonic flow and reducing the reverse flow region. The highest effectiveness has been observed in cases with fixed boundary layer separation by locating the VG closer than $100h$ distance upstream of baseline separation.

The geometry and arrangement of mVGs are critical parameters. The best performances have generally been reported with $0.2 < h/\delta < 0.5$, but effective flow separation is still possible with $0.1 < h/\delta < 0.2$. The counter-rotating mVGs have demonstrated better efficiency in 2D flow separation tests, whereas co-rotating mVGs have been found more effective in 3D separation tests. From the literature reviewed here, the most effective distance between the upstream mVGs and the baseline separation is in the range of $5h$ to $30h$.

2. Passive flow control studies in cavitation

In this section, we focus on passive techniques to control cavitation. Several methods, including geometry modification, injection, drainage, surface conditioning, obstacles, grooves, and VGs, have been proposed to attempt to passively control the boundary layer and cavitation instability effects. Table 2 summarizes the different types of cavitation to understand better the analyses reviewed in this article. The following sections present a review of studies of these different methods and their effects on cavitation. The summary overview of the methods and key results are presented in Table 3, Table 4, and Table 5.

Table 2 - a brief definition of different type of cavitation with schematics and experimental observations (a) Reprinted by permission from Springer Nature Customer Service Centre GmbH: Springer Nature, Acta Mechanica Sinica, Global cavitation patterns and corresponding hydrodynamics of the hydrofoil with leading edge roughness, Q. Chen, Y. Liu, Q. Wu, Y. Wang, T. Liu, andG. Wang, Copyright (2020), (b),(d),(e),(f), (g) Courtesy of GRENOBLE UNIV[69] and (c) Reprinted from Journal of Fluids and Structures, 39, O. De La Torre, X. Escaler, E. Egusquiza, and M. Farhat, Experimental investigation of added mass effects on a hydrofoil under cavitation conditions, 173-187., Copyright (2013), with permission from Elsevier.

Cavitation Regime	Definition and characterization	Schematic	Experimental observation [69-71]
(a) Incipient Cavitation	Beginning stage of cavitation where pressure reaches a level at or below saturation pressure and nuclei sites start to grow	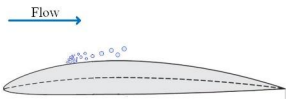	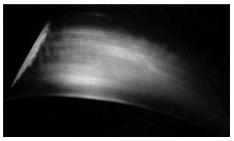
(b) Traveling Bubble Cavitation	Growth and collapse of isolated bubbles close to the surface		
(c) Attached or sheet Cavitation	Large-scale cavitation structures that form as a result of the transition from traveling bubble cavitation to one vapour-filled wake		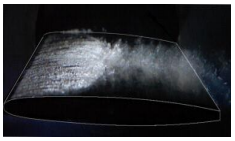
(d) Partial Cavity	An attached cavity which covers only a part of the foil		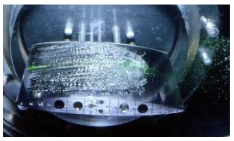
(e) Cloud Cavitation	A shedding cavity that develops when a re-entrant jet emerges from the closure region of the attached cavity and sheds by an unsteady partial cavity	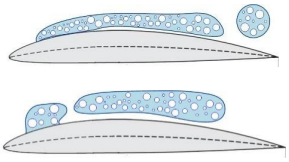	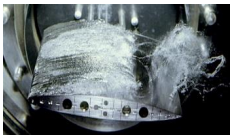

(f) Super Cavity	An attached cavity that extends over the entire suction side of the foil and closes downstream of the foil trailing edge	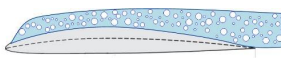	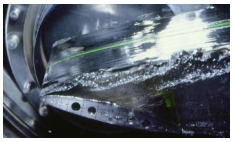
(g) Tip Vortex Cavitation	Due to the rotating motion, the static pressure at the centre of vortices drops much lower than that in the freestream, resulting in a swirling cavitation stream	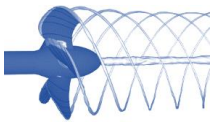	

353

354

355 ## 2.1. Surface condition and roughness

356 The properties of a solid surface, coatings, and roughness influence boundary layers, affecting heat
357 transfer and momentum transfer through the fluid-surface interface and influencing cavitation. The
358 boundary layer flow over smooth and rough surfaces is shown in Figure 10.

359 The flow over the leading edge of a smooth surface is laminar, and at some point, it becomes
360 turbulent as a result of a flow instability. A thin layer of laminar flow forms along the length of a
361 smooth surface after transiting into a turbulent boundary layer (Figure 10 (a)). Figure 10(b)
362 illustrates how roughness on the surface of a flow can cause flow instability upstream, resulting in
363 increased turbulence disrupting the viscous layer, causing the roughness layer to form, affecting
364 pressure drop and heat transfer [72]. Therefore, Boundary layer separation and cavitation can be
365 controlled by transitioning to turbulent boundary layers earlier and increasing momentum near the
366 surface.

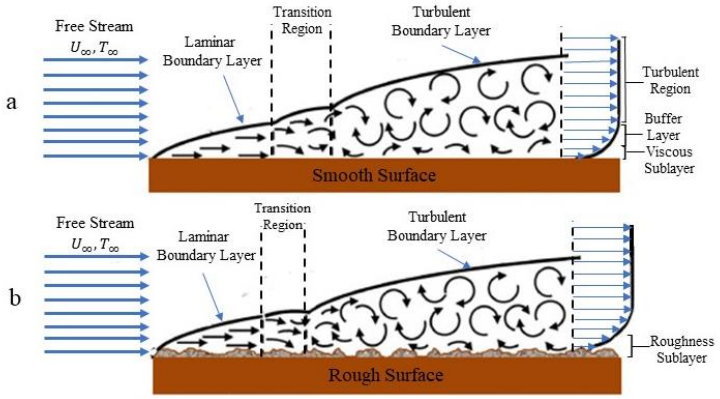

Figure 10 - Boundary layer behavior over (a) smooth surface and generating a viscous sub-layer (b) rough surface where transition to turbulent boundary layer flow happens over a shorter distance from the leading edge and with increases in instabilities and momentum transfer compared to a smooth surface [72].

The first studies which considered leading-edge roughness to investigate its effect on boundary layer separation was conducted by Dryden[73] and Kerho and Bragg[74]. Authors observed the roughness induced boundary layer transition from laminar to turbulent flow has a completely different mechanism than a natural transition in the smooth airfoil and, the roughness moved trigger of transition to, or very close, the trailing edge of the roughness. Stutz[75] investigated the influences of the roughness and divergent geometries located beneath the internal two-phase flow's cavity. The study concluded that the roughness could not significantly affect the void fraction distribution, cavity area, and time-averaged velocity. Other findings included that cavity roughness does not impact skin friction drag.

Coutier-Delgosha et al. [76] focused on the wall roughness and its effect on the unsteady behavior of the cavity flow. They observed a significant rise in the frequency of oscillations and a decline in

382 the intensity of pressure fluctuations. A significant reduction in the cavity length was also
383 observed. A study by Ausoni et al. [77, 78] examined the effects of tripping the turbulent boundary
384 layer on the wakes of blunt trailing edge symmetric hydrofoils in one specific condition. The
385 leading-edge transition was shown to promote a more organized vortex shedding with decreased
386 vortex shedding frequencies. In Figure 9, a top view visualization and measurements of vortex-
387 induced vibrations are shown. As well as confirming the tripped transition, the study also revealed
388 a significant increase in vortex-induced hydrofoil vibration and wake velocity fluctuations. The
389 span-wise organization of vortices was strengthened, as was the strength of the vortices. This
390 reduction in span-wise non-uniformities over the boundary layer was linked to the boundary layer
391 turbulent transition at the leading-edge of the hydrofoil. The study also showed how the roughness
392 induced transition led to the generation of small bubble clouds with potentially detrimental erosive
393 properties.

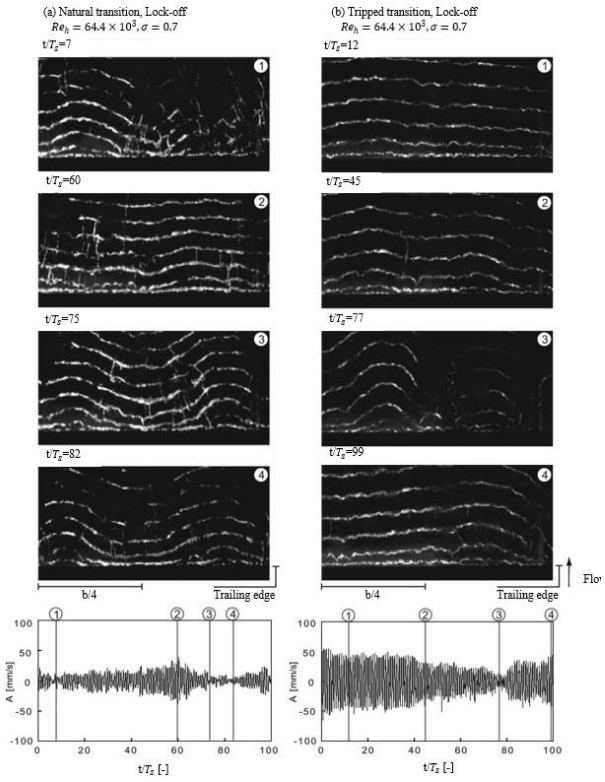

(a) *(b)*

Figure 11- Cavitation vortex street and vortex-induced vibration signal on the hydrofoil at Re=64.4×10^3 *and* $\sigma = 0.7$. *(a) Natural transition (smooth surface) and (b) tripped transition (with roughness). A direct relationship existed between span-wise vortices and vortex-induced vibration level, and with the rough surface, the span-wise vortices considerably increased in intensity and promote a re-establishment of organized vortex shedding* [78]. *Republished with permission of American Society of Mechanical Engineers ASME, from the Effects of a Tripped Turbulent Boundary Layer on Vortex Shedding from a Blunt Trailing Edge Hydrofoil, P. Ausoni, A. Zobeiri, F. Avellan, and M. Farhat, Journal of Fluids Engineering 134, (2012); permission conveyed through Copyright Clearance Center, Inc.*

The application of $15\,\mu m$ sandpaper roughness on NACA 66 hydrofoil using decreased the characteristic lift and momentum coefficients and increased the drag coefficient [79]. Petkovšek et

al. [80] investigated hydrodynamic cavitation behavior from laser-textured surfaces and found major effects on the characteristics of cavitation with sensitivity to the type of micro-structuring. By comparison against highly polished cases, the extent of cavitation was reduced with some of the laser-textures.

Emelyanenko et al. [81] implemented a super hydrophobic coating on stainless steel operating under cavitation in heavily loaded hydraulic systems. Micro- and nano-textures were developed by a nanosecond Infra-red laser and studied under long-term continuous contact with water. The hydrophobic properties and chemical stability were confirmed. Additional tests under prolonged exposure to abrasive wear and cavitation loads showed significant improvement to the functional durability.

Cavitation inception and development was investigated using hydrofoils with smooth and rough (0.4 μm) leading edges by Tao et al. [82]. According to their research, cavitation inception was enhanced by roughness when incidence angles are below 2°. The roughness element decreases wettability and traps more gas which can enhance surface nucleation and increases the risk of cavitation. In their studies of hydrofoils with high incidence angles (>3°), roughness significantly delayed cavitation incipience while developed cavitation was almost the same between smooth and rough hydrofoils. Based on their argument, this unexpected incipient delay was caused by the boundary layer structure changes due to roughness.

Churkin et al. [83] also conducted a study to determine how wall roughness impacts the cavitation structure. Under specific conditions, it has been demonstrated that varying the surface roughness type and characteristics can control the formation of cavities. Onishi et al. [84] studied the effects of hydrophilic and hydrophobic coatings on cavitation of tidal turbines and also observed that hydrophilic coating could reduce the incipient cavitation number. A lower growth of cavitation

426 was linked to the hydrophilic of textures, especially at small angles of attack. Issues related to the
427 coating lifetime with loss of effectiveness after 210 seconds of exposure to cavitation were
428 reported. Hao et al. [85] also used high speed PIV to analyze the cavitation mechanism after the
429 addition of surface roughness over the hydrofoil's entire surface. The results show that the cloud
430 cavitation mechanism changes significantly compared to smooth hydrofoil surfaces. Over a rough
431 hydrofoil, cloud cavitation appears as attached subulate cavities while cavitation over smooth
432 surfaces form finger-structured cavities. The roughen hydrofoil also experienced a longer cloud
433 cavitation period and higher cavitation growth rate.

434 Chen et al. [70] focused on the effects of localized roughness modification concentrating on the
435 hydrofoil leading edge. They observed that both lift and drag coefficients were increased by
436 surface roughening. The lift-to-drag ratio was also slightly increased and the incipient cavitation
437 number could be reduced by generating higher turbulent kinetic energy and lowering the minimum
438 surface pressure at the leading edge. The roughness did not affect however the formation and
439 transition to cloud cavitation. The change in cavitation patterns in this study is shown in Figure
440 12.

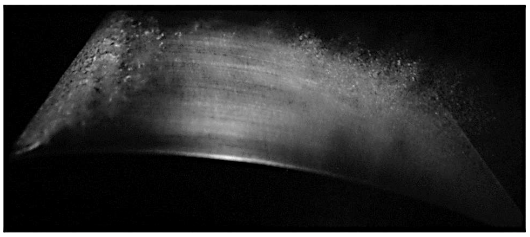

a

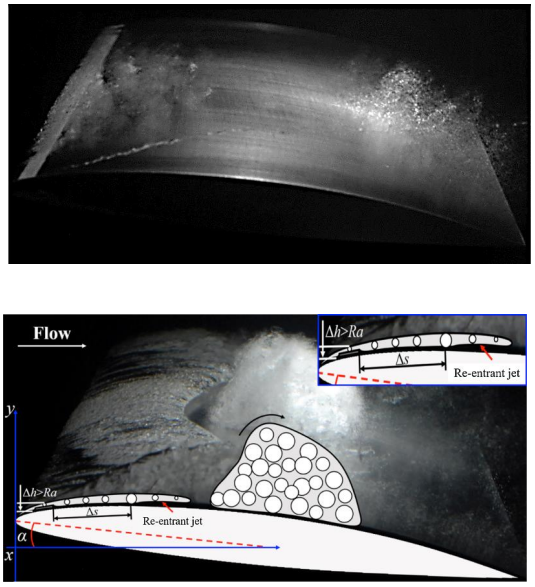

Figure 12- Cavitation patterns over a hydrofoil (a) without leading-edge roughness, with Re=0.8×10^6, $\sigma = 2.5$ and $\alpha = 8$, and observation of sheet cavitation, (b) with leading-edge roughness, with Re=0.8×10^6, $\sigma = 2.5$ and $\alpha = 8$, showing incipient cavitation and (c) with leading-edge roughness at Re=1.0×10^6, showing the formation of cloud cavitation. High-pressure gradients initiated the formation of reentrant jets toward the leading edge of the cavity during the initial stage. Thereafter, the cloud cavity characterised by a high vapor fraction, rises away from the surface when the height of the cavity (Δh) is greater than the roughness (Ra). Furthermore, there is enough distance between the leading edge roughness and the re-entrant jets (Δs), and therefore the local pressure distribution on a leading edge is greatly affected by the leading edge roughness [70]. Reprinted by permission from Springer Nature Customer Service Centre GmbH: Springer Nature, Acta Mechanica Sinica, Global cavitation patterns and corresponding hydrodynamics of the hydrofoil with leading edge roughness, Q. Chen, Y. Liu, Q. Wu, Y. Wang, T. Liu, andG. Wang, Copyright (2020).

The efficacy of a range of artificial roughness types on propeller tip vortex cavitation was also investigated by Asnaghi et al. [86]. Both of their numerical and experimental analysis showed that in the case of optimum roughness, tip vortex cavitation inception decreased around 33%, while drag force increased less than 2 % compared to the smooth hydrofoil. It is found that compared to

the smooth foil, the roughness separation line induces more distribution of vorticity over the tip, which led to the vortex strength reduction.

Svennberg et al. [87] tested two configurations of uniform and non-uniform roughness patterns of 230 μm height applied over an elliptical foil. The roughness has been shown to result in lower angular momentum one chord length downstream of the tip without notable change to the radius of the vortex core. The study found that the cavitation number for tip vortex cavitation inception can be reduced by 33 % for a 2% increase in drag by optimizing the roughness pattern. No obvious differences were noted when comparing the effect of uniform and non-uniform roughness distributions on cavitation inception properties. Non-uniform roughness distributions did, however, have a detrimental effect on drag. Also while the application of surface roughness did not increase the risk of the foil sheet cavity, it was found to impact on the small scale nuclei production. This was explained by the hydrophobic nature of the roughened surfaces, as roughness elements create nano- and micro-sized residual air pockets from which small nuclei are continuously produced as a result of local degassing.

The study of cavitation extends beyond inception and a significant research effort has been dedicated to the study of the follow on growth and collapse stages of cavitation. Published studies [88-90] have considered the effect of shock waves [91-94], refraction waves [91 95-100], thermal growth [101 95 102-109], fluids properties [107, 110, 111], and in particular liquid compressibility and viscosity [110 112 113-117] and the presence of non-condensable gas [118-120]. Not many studies however have focused on the effect of passive flow control on bubble growth and collapse. The most likely reason for this is the clearer role played by surface modification in controlling boundary layer separation than bubble growth and collapse. One notable exception is the work of Kadivar et al.[121] who recently used a rigid aluminum plate with shark skin-inspired micro-structured riblets to investigate the

effects of regular surface roughness on the bubble dynamics of a single cavitation bubble. A micro-structured V-shaped riblet was used to study the dynamics of a single laser-generated cavitation bubble. During the first collapse, microbubbles formed between the bubble and the riblet surface were shown to reduce the momentum of the micro-jet produced by the collapse. The micro structured riblets were then linked to a reduction in extent of cavitation-induced erosion. A recent study by Gonzalez-Avila et al. [122] also proposed a biomimetic gas entrapment by micro-textured surfaces (GEMS) derived from the mushroom-shaped features found in hairs and cuticles of sea skaters and springtails. The GEMS, produced by using SiO2/Si substrates and micro-fabrication techniques, were shown to trap air when immersed in water. The entrapped air, in turn, was shown to repel cavitation bubbles and protect against cavitation erosion. The process of formation, growth and collapse of cavitation bubbles is illustrated in Figure 13 with and without surface topographies. Experimental results presented demonstrated the effectiveness of the technique for a wide range of bubble to surface distances.

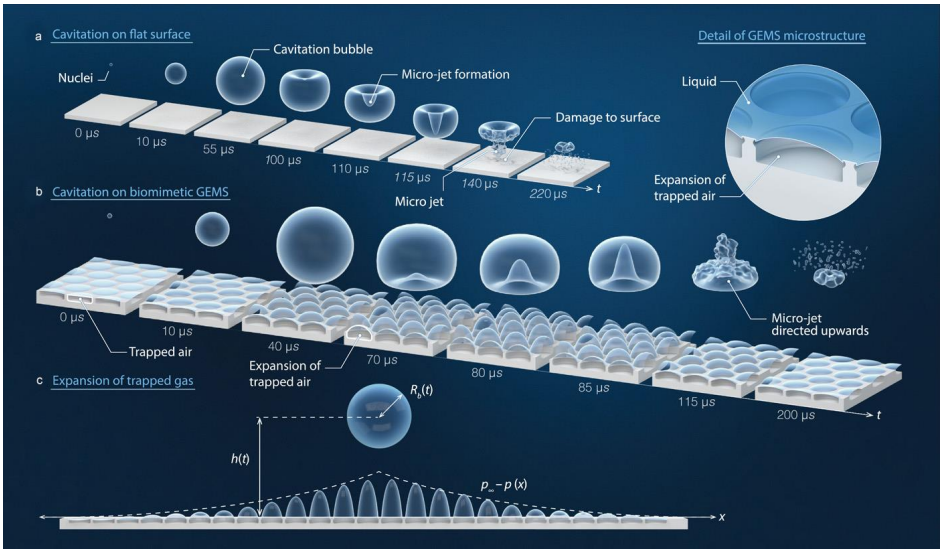

Figure 13- Gas entrapment by micro-textured surfaces as a means to prevent cavitation damage showing illustrations of (a) the cavitation process over a flat surface with a micro-jet generated from a bubble collapsing above the substrate surface which is a key factor in cavitation induced erosion, (b) the cavitation process on biomimetic Gas entrapment micro-textured surfaces, showing the entrapped gas deflecting the liquid jet's direction upward thereby protecting the surface substrate from the cavitation bubble pressure jet, and (c) the expansion of entrapped gas as a result of nearby cavitation bubble pressure field [122]. M. Nguyen, S. Arunachalam, E. M. Domingues, H. Mishra, and C.-D. Ohl, Science Advances 6, eaax6192 (2020); licensed under a Creative Commons Attribution (CC BY) license.

A summary of important studies for cavitation control using surface roughness is presented in Table 3.

2.2. Blade profile and geometry modification

Direct optimization of the blade profiles and geometries can also contribute to cavitation mitigation. Some of the earliest studies in this respect relate to efforts dedicated to the development of a series of non-symmetrical hydrofoils specifically designed to reduce the cavitation bucket in practical applications. Cavitation bucket is a diagram which can characterized the cavitation inception by presenting how minimum pressure coefficient (C_{pmin}) vary with angle of attack (Figure 14). Results indicate that a significant delay in cavitation inception could be achieved [123, 124].

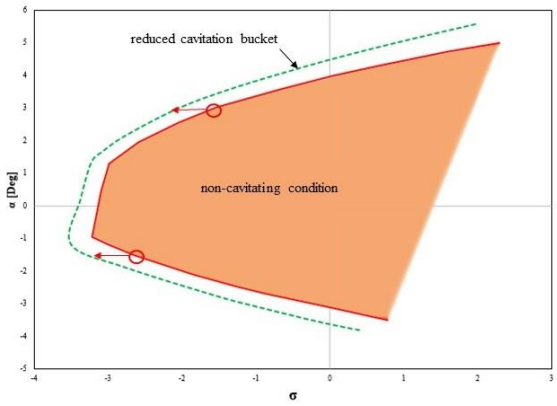

Figure 14- The cavitation bucket diagram can predict the cavitation inception based on the cavitation number or minimum pressure coefficient and angle of attack in a specific pump. Reducing or moving the cavitation bucket to a lower cavitation number can be a target as it shows a delay in cavitation inception.

Kyparissis & Margaris [125, 126] worked on different centrifugal pump blade designs, including double-arc synthetic blades and different blade leading edge angles. The investigation considered pump hydraulic performance and cavitation in tandem. The blade leading-edge angles were tested experimentally over a range of $9, 15\ and\ 21°$. For low and high angle attached cavitation was found to move from the pressure to the suction side respectively while cavitation could be eliminated $15°$ blade leading edge angle of attack. It is because the testing condition is close to that of the best efficiency point. Increasing the blade leading angle of attack in this study could increase the total head and efficiency. Other studies have documented the benefit of increasing the blade leading edge. Shi et al. [127] applied a biomimetic tubercle on the design of a tidal turbine leading-edge. They observed that the appendages could constrain the extent of the cavitation region but this was achieved at the cost of higher cavitation number and earlier onset of cavitation.

As the shape of the blade tips can have a significant effect on tip leakage, foils with various tip shapes, such as squealer tips [128-130], thickened tips [131], rounded tips [132, 133] and C-grooves [134] have been studied. The casing grooves may also serve as an effective solution for suppressing the tip-leakage vortex (TLV), according to Kang et al.[135], Hah, Choi, and Dreyer[136]. It has been confirmed however that the effect of passive control strategies in the control of tip leakage is greatly influenced by gap size [137].

The study by Custodio et al. [138] focused on the characteristics of cavitation inception with wavy leading-edge patterns. The authors found that hydrofoils with medium and large protuberances can confine the cavitation region behind the protuberance troughs. By contrast, standard hydrofoils showed sheet cavitation over the entire span. Zhao and Wang[139] conducted a numerical simulation to determine the effect of the bionic fin-fin structure on cavitation on a hydrofoil surface. Their results showed that these structures are able to increase the lift-to-drag ratio and decrease the turbulent kinetic energy and would be an effective passive control method for cavitation. A novel design for a hydrofoil with twin protuberances to mimic the two prominent tubercles found on the flipper of a humpback whale was proposed and studied by Kant and Bhattacharyya [140]. This design was characterized by its ability to limit the separation zone between the chordwise vortices shed from the two humps at high angles of attack (>20 deg). Although the pre-stall lift coefficient achieved by the modified profile was lower, the maximum lift was increased. The two protuberances were found to reduce the extent of stall separation by altering the interaction of the two chordwise vortices over the suction side, resulting in an enhanced lift after stall. At pre-stall and post-stall angles of attack, the amplitude and spacing of the two protuberances had an important impact on the lifting characteristics. It has been determined that such modifications can effectively control flow at high angles of attack and can be tailored for specific marine applications.

549 The leading-edge protuberances of humpback whale flippers were also incorporated in hydrofoil
550 modifications by Li et al. [141] to study the impact on cavitation. The wavy leading edge considered
551 improved the lift–drag characteristics, and reduced cavitation volume by around 30%. The
552 shedding of cavitation bubbles was also stabilized by reducing the wavelength and increasing the
553 amplitude of the shape modification. Increasing the amplitude significantly reduced the cavitation
554 volume, decreased the amplitude of pressure, and overall enhanced the suppression of cavitation.

555 According to a recent study of a hydrofoil with flipper protuberances on the leading edge [142], the
556 hydrodynamic performance and cavitation characteristics were significantly affected. A flow
557 visualization illustrates how the hydrodynamics and pressure distributions of modified hydrofoils
558 result from periodic and symmetric streamwise vortices that originate from protuberances. The
559 location and scale of cavitation are considerably restricted by the streamwise vortices of modified
560 hydrofoils. The relationship between pressure fluctuations and cavity evolution is also analyzed
561 with a simplified one-dimensional model. Their results showed cavity volume acceleration is
562 attributed to pressure fluctuations, which can be used to control cavitation oscillations in
563 engineering designs.

564 ### 2.3. Grooves

565 Grooves and riblets are defined as stream-wise channels on the surfaces and have been extensively
566 studied for their drag reduction properties [143-145]. They have also shown potential benefits for
567 cavitation control. A numerical and experimental study was undertaken by Li et al. [146] to examine
568 how distributed grooves affected cavitation around the body of revolution. Numerical simulations
569 showed that the grooves accentuated the pressure variations along the tunnel. Grooves also resulted
570 in significant fluctuations of pressure on the surface. According to both experimental and

numerical results, groove width was shown to affect the amplitude and interval of fluctuation and, therefore, the cavitation distribution.

Following a study on the benefit of surface roughness on unsteady shedding of cloud cavitation, Danlos, Ravelet, Coutier-Delgosha and Bakir[147] investigated longitudinal grooves and their effect on sheet cavitation. Grooves were found to suppress cloud cavitation instabilities [148]. Liu and Tan[149] studied grooves' effects on suppressing tip vortices which are precursor to cavitation inception. The analysis confirmed the ability of grooves to suppress the leakage vortices near the leading-edge of the hydrofoil subject to careful positioning.

To control TLV cavitation, overhanging grooves (OHG) were fitted to hydrofoils by Cheng et al. [150]. A significant improvement in cavitation suppression was observed with the OHG compared to the baseline, conventional grooves and anti-cavitation lip (ACL) with minimal effect on hydrofoil performance. Effective reduction in the intensity of TLVs and tip-separation vortices were achieved with small gap sizes. The OHGs were shown to increase the TLV core size when the gap size was in the medium to large range, increasing, in turn, the minimum local pressure. OHGs were also examined for their effect on hydrofoils, indicating that they can effectively suppress the fluctuation of TLV cavitation without significantly altering the time-averaged drag or lift.

2.4. Drainage and Injection

Another important family of passive flow control methods relies on drainage and injection. Kato et al. [151] developed a method based on the water discharge from a slit from the hemispherical shaped leading edge. The momentum injection created a wavy motion in the boundary layer with a wavelength higher than the boundary layer thickness. This transitional flow motion could generate an inflection in the velocity profile and disturb the separation zone. It was shown that

sheet cavitation on the hydrofoil could be suppressed completely. Arndt et al. [152] also found that the injection of air on the leading edge of a NACA 0015 hydrofoil minimized cavitation erosion.

The application of bleed and jet reinjection flow control on turbopumps were investigated by David Japikse [153]. The auto-oscillation region on the pump impeller suction surface was eliminated, and cavitation happened at a lower cavitation number, while also improving the pump's total head and efficiency, and increasing the suction's specific speed.

Zhu et al. and Bing and Hongxun [154, 155] studied gap drainage in centrifugal pump impeller as illustrated in Figure 15 (a) and (b). The approach was shown to act on cavitation while improving the pump hydraulic performance. A new type of cavitation was observed due to a change in the discharge flow due to drainage and the cavitation volume in the impeller channel.

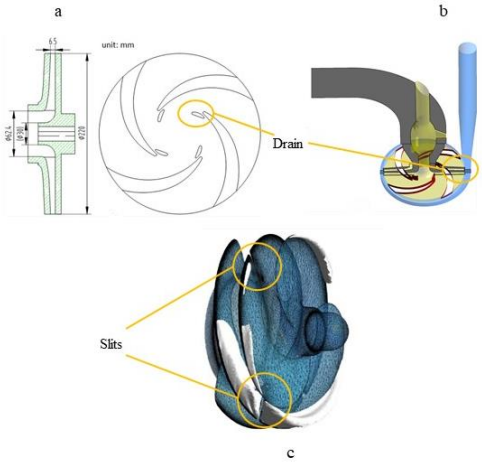

Figure 15- (a) and (b) Schematic of gap drainage impeller in Physical pump and computational region [155] Republished with permission of American Society of Mechanical Engineers ASME, from Analysis of the Staggered and Fixed Cavitation Phenomenon Observed in Centrifugal Pumps Employing a Gap, Z. Bing, and C. Hongxun, Drainage Impeller Journal of Fluids Engineering 139, (2016); permission conveyed through Copyright Clearance Center, Inc., (c) Modeling of inducer with slit under cavitation

condition [156]. Y. Kamikura, H. Kobayashi, S. Kawasaki, and Y. Iga, IOP Conference Series: Earth and Environmental Science, 240, 2019; licensed under a Creative Commons Attribution (CC BY) license.

The effect of water injection on cavitation suppression over NACA0066 hydrofoil was also investigated by Wang et al. [157]. An optimization of the position and angle of the jet were shown to have a significant effect on cavitation suppression. According to this study, this type of water injection can increase the boundary layer's velocity gradient and decrease the extent of flow separation. A decrease in the thickness of the recirculation zone and consequently of the re-entrant jets' velocity were also observed.

Kamikura et al. [156] implemented an asymmetric slit on the axial inducer's blades to observe specifically to study the effect on cavitation, as shown in Figure 14 (c). Results showed that this technique is effective on cavitation instabilities suppression while they were installed in the proper arrangement. It was observed that by viewing the flow field in a circumferential direction around the slit near the blade tip, the wave from the jet divided the cavity, which then decreased the cavity volume. Furthermore, the asymmetric arrangement of the slit in the inducer can disturb the regularity of rotating cavitation because the slit flow rates differ differently in each blade. The summary of important studies in blade profile and geometry modification, drainage and injection, and grooves and slits are presented in Table 4.

2.5. Obstacles

Early investigations of the effect of flow obstacles were precursors to VG studies. Kawanami et al. [158] studied the structure of cloud cavitation in the wake of obstacles on hydrofoils. As re-entrant jets were shown to affect the periodic shedding and generation of cloud cavitation, the obstacle on the foil was able to block the re-entrant jet off, consequently preventing the generation of cloud cavitation. In comparison with hydrofoil without obstacle, the noise intensity and hydrofoil drag

were remarkably reduced. After this seminal work, several studies have continued to explore the interaction between obstacles and cavitation instabilities [159-162]. Enomoto et al.[163] presented a study in which obstacle plates were attached upstream of helical inducers in order to suppress cavitation surges observed under partial flow conditions. Installing axi-symmetric and axi-asymmetric obstacle plates of ring type could narrow the range of the onset regions of oscillating cavitation surge. Obstacle plates with a blockage factor of 30% reduced cavitation surge oscillations to a negligible level. The suppression effects became greater with increased blockage factor. In a follow on study of inducer performance and cavitation surge suppression Kim et al.[164] considered two kinds of inducers with blade tips of 8° and 14°. The experimental study considered various axial positions of the obstacle to inducer inlet and various blockage ratios against flow passage area. A blockage of about 50% between the flow passage and the obstruction was recommended as the optimal ratio. The most appropriate axial position of the obstacle upstream of the inducer inlet must take account of the inducer blade angle with a smaller blade angle requiring a shorter distance. Axis-asymmetrical obstacles were also shown to cause vibrations even under normal operating conditions at high Net Positive Suction Head (NPSH).

Huang et al. [165] used a trip bar on an axisymmetric projectile to weaken the re-entrant jets and pressure wave propagating from the collapse of cavities. An investigation of super-cavitating flow was conducted around three different conical cavitators with wedge angles of 30 °, 45 °, and 60 ° by Kadivar et al [166]. The wedge angle of the cavitator was found to be the most effective design criteria to increase the cavity length. The results have shown that as cavitation number decreases, drag coefficient decreases, and the drag coefficient of a cavitator increases with increasing wedge angle when inlet velocity is constant. The cavity length was increased both for the lower and higher supercavitation conditions studied numerically. Che et al. [167] focused on a span-wise obstacle

located on the suction side of the hydrofoil shown in Figure 16. The near-wall pressure increased in the wake of obstacles and led to suppression of sheet cavitation. The hydrofoil modification, however, had little impact under transitional cavity oscillation most likely because of the inherently unstable flow as shown in Figure 17.

Positioning the obstacle downstream of a flat hydrofoil was investigated by Zhang et al. [168]. While no significant change in the average cavity length was observed at equivalent cavitation number, the obstacle did affect the dynamics, strength and direction of re-entrant jets.

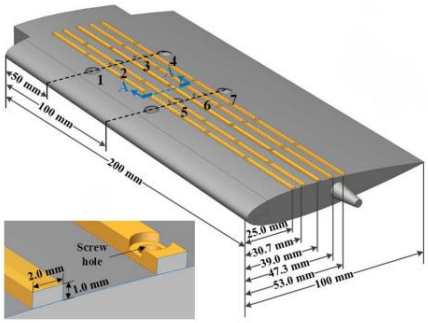

Figure 16 - Representation of Span-wise obstacles on NACA0015 hydrofoil at different positions [167]. Reprinted by permission from Springer Nature Customer Service Centre GmbH: Springer Nature, Journal of Mechanical Science and Technology, Effect of obstacle position on attached cavitation control through response surface methodology, B. Che, L. Cao, N. Chu, D. Likhachev, andD. Wu, Copyright (2019).

Using obstacles for control of baled cavitation in water jet pumps is investigated by Zhao et al. [169]. They implemented a pair of tandem obstacles on the suction side of the pump. It is observed that there is more resistance against the incipient and the development of leading-edge cavities after using obstacles. Although sheer energetic cavitation appears after obstacles with foamy wakes, pressure gradients analysis shows that these obstacles were effective in blade cavitation. However,

the hydraulic performance loss, including 6% head drop and 5.6% efficiency drop, was observed because of violent pressure fluctuations after using obstacles on the blade.

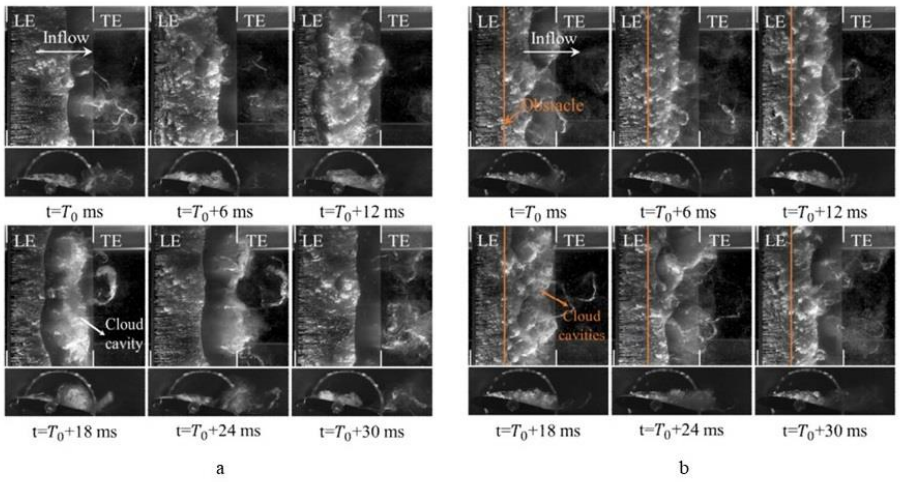

Figure 17 - (a) A typical partial cavity oscillation period on a smooth hydrofoil involves the development of sheet cavitation, the propagation of re-entrant jets, and the shedding and collapse of cloud cavities, (b) A hydrofoil with an obstacle in the same condition. The obstacle inhibits re-entrant jets during partial cavity oscillations, thereby suppressing cloud cavitation. As a result, the cavity fragments, and the cloud cavitation collapses to a non-uniform small-scale cloud [167]. Reprinted by permission from Springer Nature Customer Service Centre GmbH: Springer Nature, Journal of Mechanical Science and Technology, Effect of obstacle position on attached cavitation control through response surface methodology, B. Che, L. Cao, N. Chu, D. Likhachev, andD. Wu, Copyright (2019).

A recent study by Lin et al. [170] has analyzed the influence of arc obstacles on the evolution of cavitation over flat hydrofoils, Experimental evidence has shown that the shedding of cavitation and the distribution of air over the flat hydrofoils are influenced by the obstacles. The arc obstacles were shown to stabilize the leading edge of the shedding cavity and restrict its size, which inhibits cavitation.

2.6. Vortex and bubble generator

The ability of VGs to control boundary layer separation has been exploited on hydrofoils to destabilize attached cavities. The schematic of Figure 18 [171] illustrates how counter-rotating vortices generated upstream of the cavity by the VG delays separation and promotes the formation of a smaller cavity with a growth and shedding behavior similar to the attached cavity generated by laminar boundary layer separation but with some important distinction. Its leading edge is observed to move dynamically, likely due to a thin liquid layer separating the cavity from the wall as conjectured by the authors and the cavity edge shows oscillations indicative of a turbulent flow.

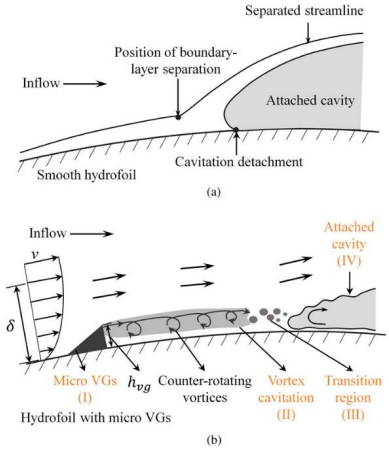

Figure 18-Schematic description of attached cavitation over (a) a smooth hydrofoil; a typical process of attached cavitation formation and (b) a hydrofoil with micro-vortex generators where (I & II) every standalone micro-vortex generators induces counter-rotating vortices at the end of their trailing edge and develop micro-vortex cavitation, (III) a narrow transition region exists between vortex cavitation and attached cavitation, which is caused by shedding of several small bubbles produced by vortex cavitation, and then in (IV) attached cavitation is developed without glossy and divot structures observed in smooth hydrofoil [171]. Reprinted from Control effect of micro vortex generators on leading edge of attached cavitation, B. Che, N. Chu, S. J. Schmidt, L. Cao, D. Likhachev, and D. Wu, Physics of Fluids 31, 044102 (2019) with the permission of AIP Publishing.

The low-pressure core of the stream-wise vortices induces stable vortex cavitation which breaks down into bubble clouds upstream of the attached cavity. Similar observations were made in a study of VGs by An [172]. The application of VGs in control of cavitation in multi-propulsion vessels was studied by Liang-mei[173]. They found a significant improvement in cavitation instability and declining pressure fluctuation.

The application of bubble generators on cavitation control was studied by Javadi et al. [174] through a two-dimensional cavitation calculation. This bubble generator was actually a wedge type VG. Their numerical analysis showed that this VG can make a low pressure recirculation region (below saturation pressure) behind the VG. Bubbles then start to generate and grow in this region. By controlling this condition, the bubbly flow becomes stable and will not vanish, or in other words, interfere and stope the cavitation process. They observed that the whole cavitation process, including vaporization, bubble generation, and bubble implosion, could be affected, and lift and drag fluctuations could be reduced.

Vortex generators that have been optimized can also be used for TLV cavitation suppression. The experimental results of Amini et al.[175] have shown that the winglets could effectively increase the radius of the tip vortex, and delay the initial inception of the TLV cavitation process. The ACL, however, is the only proposed method that has actually been applied. Results showed that it is difficult for the ACL to have a satisfactory inhibitory effect on TLV cavitation and once the vortex generators are not operating under design conditions, a more intense level of cavitation will be induced [137, 176].

A recent numerical study by Kadivar et al. [177] proposed a new type of VG called Cavitating bubble Generators (CGs) (Figure 19). The CGs were adopted from wedge-type VGs were used before for aerodynamics application with the aim of generating cavitating bubbles at the suction side of

hydrofoil. They observed that high momentum fluid from free stream flow moved to the hydrofoil's near-wall low energy region. These CGs could generate vortices downstream and move higher kinetic energy flow to the vicinity of the hydrofoil surface. Consequently, quick high-pressure pulsations near the hydrofoil surface were reduced, and the resistance against pressure rise before boundary layer separation was increased. They found the vortex structures were significantly modified on the suction side and the hydrofoil wake region. This phenomenon suppresses the cyclic behavior of unsteady cloud cavitation and declining turbulent velocity fluctuation in that area. The experimental investigation of CGs proved an essential role of re-entrant jets on cloud cavity shedding structure [178]. Their experiment proved the reduction of pressure pulsation's amplitude in instabilities of cavitation dynamic. As a result, they can be used as a useful tool for delaying cloud cavitation formation. A comparison between hydrofoil with and without CGs is presented in Figure 20. In another study, a CG was installed adjacent to the cavitation inception on a semi-circular leading-edge flat plate to control and manipulate unsteady dynamics of cavitation surge. The CG was shown to mitigate large-scale cavities, suppress the spanwise instability of adjacent cavities, and suppress large-scale cavities over the flat plate. Passive control was observed to reduce the dominant frequency of pressure pulsations[179].

Xu et al. [180] used cavitators placed at various locations on a hydrofoil's bottom surface to study the supercavitation flow around it. As their observations showed, a localized high-pressure region appears between the leading edge of the hydrofoil and the cavitator, and downstream of the cavitator, the pressure is equal to the saturated vapour pressure of water. Based on the magnitude and distribution of pressure on the hydrofoil surfaces, the lift coefficient increased as the cavitator was positioned farther away from the leading edge and towards the trailing edge. Alternatively,

747 there was a strong correlation between drag coefficients and the maximum thickness of cavitating
748 wakes, which was used as a proxy for the drag coefficient.

749 Kadivar et al. [181] also examined a single span-wise row of cylindrical obstacles named Cylindrical
750 Cavitating bubble Generators (CCGs), shown in Figure 21. Similar effects were observed such as
751 a reduction in the adverse pressure gradient at the end of cavity, weakening of re-entrant jets and
752 turning unsteady cavity structure to a quasi-stable cavity structure. As a result, the instability of
753 cloud cavitation was mitigated and the near-wall high-pressure pulsation dampened. One key
754 difference to previously studied CCGs is that only small-scale cavity structures are shed while
755 large-scale cavitation clouds are effectively suppressed. It was also observed that vibration-
756 induced cavitation as well as wall-pressure peaks on materials with solid surfaces were
757 significantly reduced [181] [182]. In another study, high-speed visualization, PIV and a hydroacoustic
758 pressure transducer were used to analyze experimentally the effects of CCGs on turbulence
759 behavior, the amplitude-frequency spectra of pressure pulsations associated with oscillations in
760 the attached cavity length and cloud cavitation instabilities. This study confirmed that CCGs is
761 quite effective at hindering the development of cloud cavitation and at decreasing the strength of
762 middle- and side-entrant jets which are the primary mechanism that cause unstable cloud cavitation
763 [183].

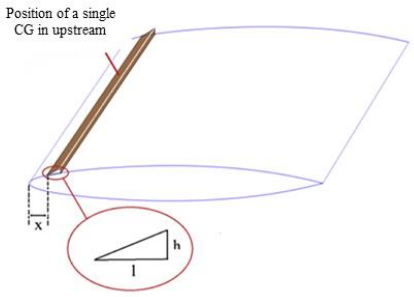

Figure 19 - Analysis of wedge-type Cavitating bubble Generators located on the suction side of a hydrofoil was found to reduce high-pressure pulsations, alter boundary layer separations, and alter vortex structures [177]. Reprinted from Applied Mathematical Modelling, 64, E. Kadivar, O. e. Moctar, and K. Javadi, Investigation of the effect of cavitation passive control on the dynamics of unsteady cloud cavitation, 333-356., Copyright (2018), with permission from Elsevier.

Che et al. [171] considered counter-rotating delta-shaped mVGs built into a quasi-two-dimensional NACA0015 hydrofoil (Figure 22). The type and geometry of mVG was based on designs from Lin[26] and Godard and Stanislas[37] reviews to control boundary layer separation using VGs [184]. They designed five counter-rotating delta-shaped mVGs with different h/δ in the range of 0.5 to 2.5. The ΔX_{VG} were set at 2.5 mm from the hydrofoil leading edge based on the position of boundary layer separation at the leading edge obtained from their 2D numerical modeling results. The study demonstrated that the mVG can suppress the laminar separation under non-cavitating conditions. MVGs located within the viscous sub-layer close to the cavitation detachment point failed to suppress the attached cavitation. Results did show however that the transition region and attached cavitation were affected. The authors found that at lower heights relative to the viscous sub-layer, mVGs can generate longer counter-rotating and cavitating vortices within the boundary layer. These mVGs could also fix cavitation inception causing more stable sheet cavitation and cloud cavity shedding. The attached cavitation over the smooth hydrofoil showed a formation of "divot"

or “finger” structure as well as two-dimensional Tollmien–Schlichting waves which are shown in Figure 23. Divots are three-dimensional flow structures which appeare near the cavity interface. They occur at moderately high Reynolds numbers because of local disturbances near cavity interfaces. Upstream of the detachment point, local disturbances were caused by a breakdown of the laminar boundary separation, resulting in a divot when a jet of fluid penetrated the cavity [19]. Tollmien–Schlichting waves are known as stream-wise instabilities that occur prior to the transition to turbulence in boundary layers. This instability initiates because of the interaction of disturbances with leading edge roughness and can be slowly intensified while moving downstream and can help with the process of turbulence transition [185]. In comparison with a smooth hydrofoil surface, cavitation started closer to the leading edge, eliminating classic "fingering structures" and Tollmien-Schlichting waves [184].

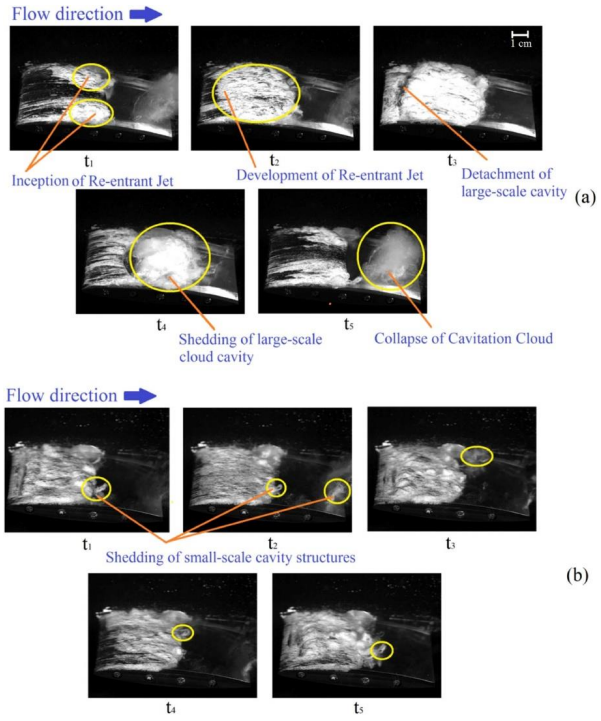

794

795 *Figure 20- Structure of cavitation over a hydrofoil with attack angle of* $7°, \sigma = 1.3$ *and* $Re = 1.4 \times 10^6$*. (a) CSmooth hydrofoil:*
796 *t_1&t_2) Formation and development of sheet cavities and jets, t_3) detachment of large-scale cavities, t_4) shedding of large-scale*
797 *cavitation clouds, t_5) collapse of cavitation clouds. (b) Hydrofoil with cavitating bubble generators: inception and shedding of*
798 *small vortex cavitation over hydrofoil and suppressing could cavitation [178]. Reprinted from Control of unsteady partial cavitation*
799 *and cloud cavitation in marine engineering and hydraulic systems, E. Kadivar, M. V. Timoshevskiy, M. Y. Nichik, O. el Moctar, T.*
800 *E. Schellin, andK. S. Pervunin, Physics of Fluids* ***32****, 052108 (2020) with the permission of AIP Publishing.*

801

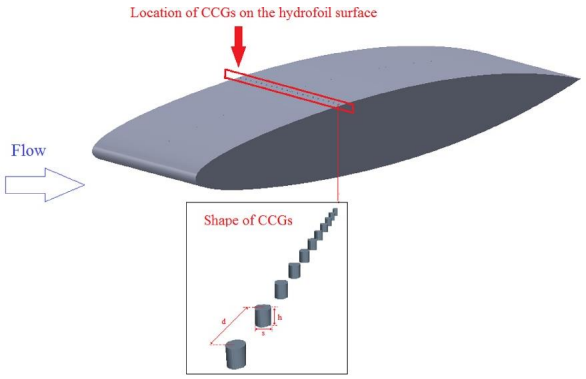

802

803 *Figure 21 - Hydrofoil with cylindrical cavitating bubble generators located on the suction side where s, h, and d are the diameters,*
804 *heights, and distances between cylindrical obstacles, respectively. Cylindrical cavitating bubble generators were investigated at*
805 *locations downstream and upstream of the hydrofoil suction surface. Using the cylindrical cavitating bubble generators, significant*
806 *reductions were seen in cavitation induced vibration, high wall pressure peaks, and cloud cavitation instability [181]. Reprinted from*
807 *International Journal of Multiphase Flow, 115, E. Kadivar, O. e. Moctar, and K. Javadi, Stabilization of cloud cavitation*
808 *instabilities using Cylindrical Cavitating-bubble Generators (CCGs), 108-125, Copyright (2019), with permission from Elsevier.*

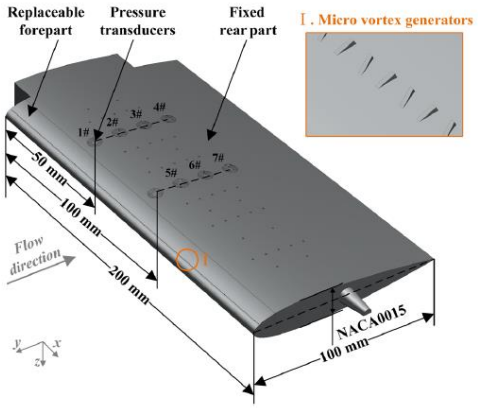

809

810 *Figure 22 - Schematic of the test hydrofoil with micro-vortex generators. The vortex generators are microscopic delta-shaped*
811 *counter-rotating vortex generators installed at the leading edge, which were shown to effectively manipulate boundary layer and*
812 *cavity dynamics in the test [171]. Reprinted from Control effect of micro vortex generators on leading edge of attached cavitation, B.*

*Che, N. Chu, S. J. Schmidt, L. Cao, D. Likhachev, and D. Wu, Physics of Fluids **31**, 044102 (2019) with the permission of AIP Publishing.*

They observed a new structure for cavitation onset while the cavitation onset disappears close to the laminar separation. In the new structure, stable vortex cavitation and subsequent vortex breakdown resulted in bubbly structures, which was finally expressed as an attached cavity region. This vortex break-down was delayed when they reduced the height of mVGs. This delay resulted in a rise in cavitation vortex pattern length. This result showed the potential of mVGs in control of cavity dynamics considering the re-entrant jet penetration depth. The flow visualization of attached cavitation during cloud cavitation without and with VGs in this study is presented in Figure 23 and Figure 24.

In another study, Che and co-authors analyzed the instability of the attached cavitation produced with mVGs [186]. This study confirmed that these mVGs are an effective passive control for attached cavitation dynamics and changed the surface wall's vicinity's flow dynamics. The results also emphasized again that the mVGs could increase the cavity length and induce counter-rotating stream-wise vortices. The mVGs could change the sheet cavity structure to a uniform cavity in a span-wise direction by inducing consistent separate vortex cavitation streaks. The mVGs showed their ability to fix the attached cavitation inception line location, thereby limiting instabilities caused by span-wise disturbances.

In this study, Che et al. [186] interpret two types of Rayleigh–Taylor (R-T) and K-H instabilities, while cavity shedding and re-entrant jets interactions happened over a smooth hydrofoil and hydrofoil with mVGs. Re-entrant jets are generated by exposing cavity closure to an adverse pressure gradient. After propagating upstream, these re-entrant jets impact the cavity interface, causing the cavity to shed. It is possible to interpret the interaction of re-entrant jets and cavities

as an R-T. A re-entrant jet and cavity interface at the leading edge interact, generating several cavitating vortices that are indicative of the K-H instability. The K-H instability interpretation has been explained by different shearing velocities causing cavity shedding.

Che et al. [186] presented evidence that reverse flow beneath the attached cavities which were linked to R-T and K-H instabilities were suppressed. The mVGs were shown to influence partial cavity oscillations, transitional cavity oscillations, and transition between these two instabilities. Experimentation was extended to measure cavitation erosion and analyse impulsive loading from cavity collapse as a measure of the intensity and aggressiveness of cavitation structure with mVGs [187]. The study also included an analysis of the dynamic behavior of the re-entrant jet, shown in Figure 25. The effect of the mVGs included suppression under certain condition of periodic shedding, and reduction of the maximum pressure fluctuations and associated acoustic power. The arrangement and geometry were shown to be an important factor in determining leading-edge erosion which was shown to increase at lower angles of attack.

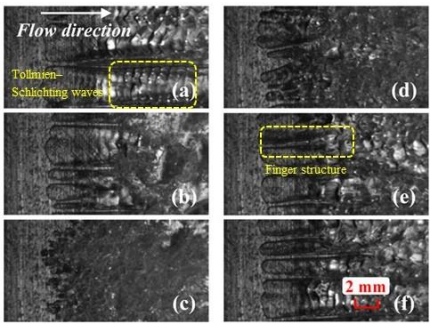

Figure 23 - (a)-(f) Dynamics of cloud cavitation shedding on a smooth hydrofoil. At the leading edge of attached cavitation, typical finger structures are visible. By observing the glossy

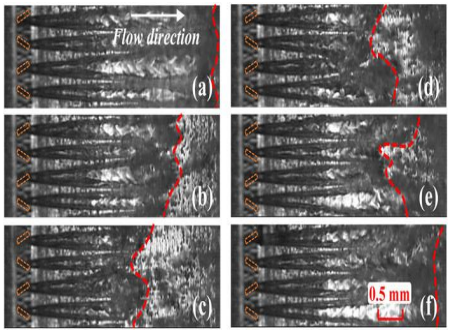

Figure 24-(a)-(f) Dynamic behavior of vortex cavitation on a hydrofoil with micro-vortex generators, with dashed boxes and dashed lines indicating the position of vortex generators

interfaces of the cavity and the Tollmien-Schlichting waves at the leading edge, laminar separation can be detected. A consistent change in finger structures resulted in cloud cavitation shedding and instability. Cavity collapse occurs when the re-entrant jet propagates upstream and reaches the leading edge. [171]. *Reprinted from Control effect of micro vortex generators on leading edge of attached cavitation, B. Che, N. Chu, S. J. Schmidt, L. Cao, D. Likhachev, and D. Wu, Physics of Fluids* ***31****, 044102 (2019) with the permission of AIP Publishing.*

and the trailing edge of vortex cavitation, respectively. As shown in the picture, classical finger structures and Tollmien–Schlichting waves have been eliminated. The cavitation onset moved toward the leading edge, which happened at the laminar separation line for smooth hydrofoil. The onset cavitation mechanism includes stable vortex cavitation, which breaks down to a bubbly structure and accumulates in an attached cavity region.[171]. *Reprinted from Control effect of micro vortex generators on leading edge of attached cavitation, B. Che, N. Chu, S. J. Schmidt, L. Cao, D. Likhachev, and D. Wu, Physics of Fluids* ***31****, 044102 (2019) with the permission of AIP Publishing.*

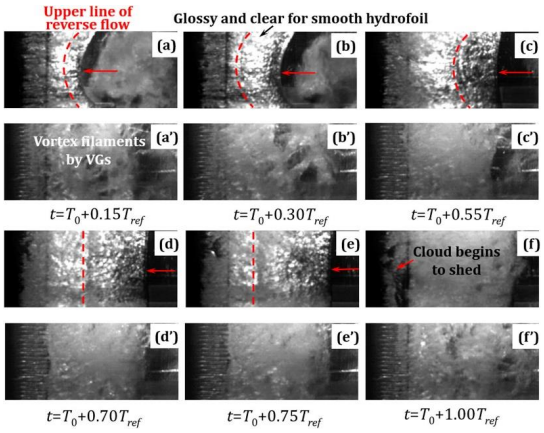

Figure 25- Behavior of re-entrant jets (α = 8○, U_∞= 10 m/s, and σ = 1.7) on (a)-(f) smooth hydrofoil and (a')-(f') Hydrofoil with vortex generators. For hydrofoil with vortex generators, downstream travelling vortices break the regular movements of re-entrant jets and suppress them. The cavity is confined and does not form a cloud, and the consequent collapse is not strong enough [187]. *Reprinted from Effects of microvortex generators on cavitation erosion by changing periodic shedding into new structures, N. Qiu, W. Zhou, B. Che, D. Wu, L. Wang, and H. Zhu, Physics of Fluids 32, (2020) with the permission of AIP Publishing.*

855 The application of mVGs has started to be investigated in applications other than 2D hydrofoil.
856 Examples include Huang et al. [188] study. They investigated the effects of VGs on cavitation in
857 marine shipping. The VGs studied could lead to more uniform wake and milder propeller
858 cavitation. These VGs could decrease pressure fluctuations and cause a more uniform distribution
859 of energy. Li et al. [189] designed a delta-shaped VG to solve the vibration problem in the hull
860 propeller and improve the ship wake quality and uniformity. The VG design was based on the
861 ship body lines. It improved the wake uniformity in certain positions as it could generate a more
862 moderate circumference transition and effectively increase the velocity in high wake areas.
863 Additionally, the VGs were able to smoothly transition the unsteady cavitation of the blade in
864 circumference direction and decrease the amplitude of pressure fluctuations. The distance between
865 the positions of blade cavitation collapses, and ship bottom shell was increased after using VGs.

866 Teplov and Lomakin[190] used computation simulation to examine mVGs located at the front edge
867 on the suction side of impeller blades in a centrifugal pump and analyzed their effect on the
868 cavitation characteristics, efficiency, and pump head. The NPSH was significantly decreased, and
869 the pump efficiency above the Best Efficiency Point was increased.

870 A study published recently by Chen et al.[191] investigated the effects on cavitation of two schematic
871 designs of mVGs around a NACA66 hydrofoil. Two different sets of mVG were installed and
872 positioned upstream of (mVG-1) and within (mVG-2) the laminar separation zone of the baseline
873 hydrofoil. The experimental results indicated that the mVG-1 could promote inception of
874 cavitation earlier than the baseline hydrofoil, while mVG-2 delayed cavitation inception especially
875 at small angle of attack cases. Two reasons were suggested for the effect of the mVG-1. The mVG-
876 1 modification was shown to generate fingerlike vortex at its rear which was observed before in
877 previous studies [85, 171, 184] and is shown in Figure 23. These vortexes were responsible to induce

878 fingerlike vortex cavitation. In addition, the mVG-1 increases the length of the laminar separation
879 bubble (LSB), resulting in laminar boundary layer separation with a lower pressure minimum.
880 Since mVG-2 was located in a high pressure zone from the leading-edge, there are insufficient
881 downstream fingerlike vortices to induce cavitation which can reduce LSB length. Smaller LSB
882 was able to suppress cavitation at $\alpha = 6°–8°$. A summary of studies in the field of obstacles and
883 VGs in cavitation control studies is presented in Table 5.

884

885 *Table 3- Summary of research for implementing Roughness as a surface methodology technique in cavitation control*

Investigator(s) (year)	*Type of modification*	*U_∞[i] (Re)*	*α [ii]*	*σ [iii]*	*Coating roughness*	*Cavitation regime*	*Comments*
Coutier-Delgosha et al. [76] (2005)	Wall roughness on a Two-dimensional foil (c^{iv} =150mm,S^{v} =80 mm)	6 m/s	0– 6°	0.7–1.8	$100, 200, 400\ \mu m$	*Cyclic Cloud Sheet cavitation*	↓ cavity length ↑ oscillation frequency ↓ pressure fluctuation intensity
Ausoni et al. [77, 78] (2007&2012)	*Blunt trailing edge on NACA* 0009 *Hydrofoil* ($c = 100\ mm, S = 150\ mm$)	(16.1×10^3 – 96.6×10^3) (42×10^3 – 70×10^3)	0°	NA	$125\ \mu m$ ($\frac{\Delta x}{c} = 4\%$) *Width* = 4%	*Vortex shedding*	↑ organized vortex shedding ↓ vortex shedding frequency ↑ vortex span-wise organization ↑vibrations induced by vortices ↑vortex strength and wake velocity fluctuations generates many tiny bubbles which may be erosive in turbomachines
Onishi et al. [84] (2017)	Hydrophilic and hydrophobic coatings on symmetrical $NACA16-021$ ($c = 40\ mm, S = 60\ mm$)	$3\frac{m}{s}$ (1.1×10^5), $5\ m/s$ (2.0×10^5)	10°, 14°, 20°	0– 4.5	$3 \sim 4\ \mu m$	Tip Vortex Cavitation, Sheet Cavitation and Cloud Cavitation	↓ Incipient cavitation number ↓Cavitation growing for in hydrophilic coating Losing Functionality after 210 seconds of cavitation condition for both hydrophilic and hydrophobic coatings
Hao et al. [85] (2018)	Surface roughness on Clark-Y hydrofoils ($c = 70mm$)	$8m/s$ (5.6×10^5)	8°	0.87, 1.02	$6.9\ \mu m$	Cyclic cloud	Change in development of cloud cavitation ↑ Intensity of cavitating flow around the rough hydrofoil

Chen et al. [70] (2020)	Surface roughness on NACA 66 hydrofoil ($c = 100\ mm, S = 149\ mm$)	$6 - 14\ m/s$ ($0.6 - 1.4 \times 10^6$)	-12 – 12 °	1– 5.5	$150\ \mu m$. ($\frac{\Delta X}{c} = 4\%$) $Width = 4\%$	Inception Sheet Cloud	↑Lift, drag and lift to drag ratio ↑ Minimum pressure coefficient No effect on cloud cavitation formation
Svennberg et al. [87] (2020)	uniform and non-uniform roughness patterns on elliptical foil (c=126.5mm, S=300 mm)	6.8 m/s (8.95×10^5)	9°	NA	h=230 µm	Tip vortex cavitation	↓Cavitation number for tip vortex cavitation inception ↑Drag force ↑Nano- and micro-sized residual air pockets

[a] Free-stream stream-wise velocity

[b] Angle of attack

[c] Cavitation number

[d] Hydrofoil chord

[e] Hydrofoil Span

Table 4- Summary of research for blade profile and geometry modification, Drainage and Injection and grooves and slits as surface methodology techniques in cavitation control

Investigator(s)	*Type of modification*	$U_\infty(Re)$	α	σ	*Geometry properties*	*Cavitation regime*	*Comments*
Blade profile and geometry modification							
Custodio et al. [138] (2018)	Protuberances on the humpback Sinusoidal pattern	$7.2\ m/s$ (7.2×10^5)	$-12 - 30°$	$\sigma\_in = 0 - 9$	Protuberances amplitude= 0.025, 0.05 & 0.12 c	Sheet cavitation	Confining the cavitation to the region behind the protuberance with medium and large protuberance amplitudes Improving the sheet cavitation pattern.

	on NACA 634-021 profile (c=200 mm)				Protuberances wavelength: 0.25, 0.5 c		
Zhao and Wang [139] (2019)	Bionic fin–fin structure on 2D NACA 0015 (c=100 mm, S=100 mm)	10 m/s (1×10^6)	8°	0.8	Rectangular fins, width= 2 %c distance of the two symmetric structures = 20% C, the inclination angle is 14 front distance of the symmetrical structure is 50%	Cyclic cavitation	↓Turbulent kinetic energy of the hydrofoil ↑lift-to-drag ratio
Petkovšek et al. (2018) [80]	Laser-textured surfaces on stainless steel cylinders (diameter =10 mm)	Flow rate: $163 - 231\ L/s$	NA	1.2–2.2	Micro-channels width: 100 µm four different angles (0°, 18°, 45°, 72°) distance between channels: 200 & 500 µm Micro-holes: diameter: 40 µm distance between holes: 200 µm	NA	↓Cavitation extent ↓Cavitation incipient number
Kant and Bhattacharyya [140] (2020)	twin-protuberance NACA 63_4-021 hydrofoil (c=100 mm, S=200mm)	2 m/s (2×10^5)	5-25	NA	twin-protuberance hydrofoil design mimicking the two prominent tubercles present on a humpback whale flipper	NA	limit the separation zone between the chord wise vortices shed from the two humps at high angles of attack (>20º). ↓ Pre-stall lift coefficient ↓ Stall separation, ↑Lift after stall. effectively control flow at high angles of attack
Li et al. [141] (2021)	Bionic NACA 63_4-021 hydrofoil with a wavy leading-edge (c=102 mm, S=204mm)	7.2 m/s (7.2×10^5)	18º	NA	Design inspired from pectoral fin of humpback whales, sinusoidal with amplitude = 0.05c & and wavelength = 0.5c	Attached cavitation Cloud Cavitation	↑Improves lift–drag characteristics ↓Cavitation volume by around ↓Pressure amplitude Enhances cavitation suppression Restrains hydrofoil cavitation
Drainage and Injection							
Arndt et al. [152] (1995)	Air injection on NACA 0015	20 m/s	8°	0.5– 6	5 holes with 5 mm distance from each other and	Sheet cavitation	Effectively minimizes cavitation erosion

	(c=81 mm, half S=95mm)				0.5 mm diameter		
Zhu et all. [154] (2014) Bin et all. [155] (2016)	Gap impeller on pump's blades (Cylindrical 2D blades for a LSSCP)	17.3 m/s (45×10^3)	NA	0– 1	Pump: 4 gad impellers Rotating speed = 1000 rpm Water head =7 m	Cloud cavitation	↑Pump's hydraulic performance and cavitation resistance Suppressing generating cavitation A new cavitation regime with different attack angles was developed allocated flow discharge and cavitation volume affects this new cavitation structure
Wang et al. [157] (2017)	Water injection on NACA0066 hydrofoil (c=150 mm)	5.33 m/s (0.8×10^6)	6,8°	0.55 − 1.0	Jet hole diameter: 2mm Injection position: 10-90 %c	Cloud cavitation	Water injection angle and jet angle affect cavitation suppression ↑ Boundary layer velocity gradient and enhance anti-reverse pressure gradient ↓ Recirculation zone thickness ↓ Velocity of the re-entrant jet ↓ Intensity of separation flow
Kamikura et al. [156] (2019)	Asymmetric slits on each blade of Inducer 335	NA	NA	0.01 − 0.3	Slit depth 30 mm Slit width 5mm Inducer speed = 6,000rpm	Vortex Cavitation	↓ Cavity volume Suppressing cavitation instabilities by rearranging the asymmetric slits
Groove and slit							
Li et al. [146] (2009)	Distributed grooves on MK46 torpedo (c=120mm)	25 − 30 m/s	NA	NA	Groove width: 3-10.5 mm Groove depth: 1.5 mm Number of grooves: 9-28	Cyclic cloud	Effect on the cavity clouds' position and shape depends on grooves' dimensions ↑ Pressure fluctuation ↑ Pressure drops in certain local regions which may increase the possibility of enhance cavitation inception ↓the stability of the cavities because of pressure fluctuation
Danlos et al. [147-148] (2014)	Longitudinal grooved surfaces on a Venturi	~$8m/s$ ($5.2, 5.5 \times 10^5$)	NA	1– 1.8	d= 1,2 mm h= 0.25,2 mm N= 40-124	Sheet cavitation Cloud cavitation	↓ Shedding of unsteady partial cavitation ↓ Surface erosion Suppressing the cloud cavitation shedding

							Grooves geometries affects cavitation regime One of the determining factors is depth of grooves Large depth of grooves can modify the sheet cavity structure No change in sheet cavity length with groove's depth smaller than viscous sublayer thickness
Cheng et al. [150] (2020)	overhanging grooves attached to the f d NACA0009 hydrofoil tip (c=100mm)	10 m/s	10 °	2	attaching several tabs, connected with each other by a slender beam with gap of 2,7&20 mm	Tip-leakage vortex	More suppression for small gaps OHGs with small gap sizes can weaken the strength of both TLV and tip-separation vortex ↑in the TLV core size ↑local minimum pressure limiting influence on the performances of hydrofoil in a large range of the gap sizes

893

894 *Table 5- Summary of research for obstacles and vortex generators studies in cavitation control*

Investigator(s)	*Type of modification*	U_∞ (Re)	α (º)	σ	h $[mm]$ (h/δ)	$\Delta X_{VG}/c$ $(\Delta z/c)$	*Cavitation regime*	*Comments*
Obstacles								
Kawanami et al. [158] (1997)	An obstacle on an Elliptic Nose Foil (c=150 mm & S=150 mm)	Propeller tunnel $5.0\ m/s$ (7.2×10^5) For TE tunnel $7.5\ m/s (8.6 \times 10^5)$	6	Propeller tunnel: 1.07 TE tunnel:1.72	2 (width 2mm)	37% c 60% c	Cyclic Cloud	Holding back the re-entrant jets ↓ Cloud cavitation ↓Noise Intensity ↓Cavitation drag coefficient

Pham et al. [159] (1999)	Obstacle on the flat ($c = 150\ mm, S = 80mm$)	$8\ m/s$ (1.2×10^6)	3, 3.25, 3.5	0.94	2 (width $4mm$)	23.3% c	Cyclic Cloud	Cloud cavitation control Holding back re-entrant jets
Sato et al. [160] (2002)	Obstacle on the flat hydrofoil (c= 70 mm, S=70mm)	$3.59\ m/s$	3.8	0.8, 1.0	3 ($width\ 3mm$)	33% c	Cyclic Cloud	No change in frequency or magnitude of oscillation
Zhao et al. [161] (2010)	Obstacle on the NACA0015 hydrofoil (c=100 mm)	(1×10^6)	8	1.2, 1.5	1, 2 ($width\ 2mm$)	32, 37 , 45% c	Cyclic Cloud	↓ Lift and drag force ↑ lift to drag ratio ↓ Cloud cavitation Restraining re-entrant jets
Ganesh et al. [162] (2015)	Venturi wedge ($c = 241.3\ mm$ $, S = 76\ mm$)	$8\ m/s$	22.1	1.81 − 1.94	4 (Width 4 mm)	26.1% c	Cyclic Cloud	↓ Void fraction in the cavity ↑ Cavity length
Zhang et al. [168] (2018)	$Obstacle\ on\ the\ flat\ hydrofoil$ ($c = 150\ mm$, $S = 200mm$)	$10\ m/s$	0	0.68 − 0.76	2 (width 2mm)	37%c	Shedding cavitation Cloud cavitation	Constant average cavity length Changing the transient re-entrant jets in terms of strength and direction
Che et al. [167] (2019)	Span-wise obstacle on the 2D NACA0015 hydrofoil ($c = 100\ mm$,	$6\ m/s$	6.5 − 8	0.8 − 1.7	2 (Width 2mm)	25, 30.7, 39, 47.3, 53 %c	Sheet cavitation Sheer cavitation	↓Sheet cavitation ↑ Pressure in the near-wall region ↓ Energy flux, cavity length, and acoustic intensity

	$S = 200$)							Cloud cavitation control Cannot suppress cavitation under transitional cavity oscillation
Lin et al. [170] (2021)	different-sized arc obstacles on a f flat hydrofoil (c=100mm)	14 m/s	5	1	convexity of the arc = radius/5= 1-2.4 mm	NA	Cloud Cavitation	↓Shedding cavity size ↑Shedding frequency as arc radius increase Stabilize the frequency of shedding cavity on the leading edge Transforming the large-scale shedding to the small-scale shedding at the trailing edge as arc radius increase
Vortex Generators								
Javadi et al. [174] (2017)	Artificial cavitation bubble generator on hydrofoil CAV2003 (c=100mm)	6 m/s	7°	0.4 – 4	0.367 mm	NA	Periodic cloud shedding	↓Lift and drag fluctuations Producing low-pressure recirculating area Inducing stationary cavitation bubbles Controlling parameters: the location, shape, and size of VGs are the crucial
Kadivar et al. [177] (2018)	Wedge-type cavitating bubble generators on CAV2003 benchmark	6 m/s (6 $\times 10^5$)	7°	0.8	0.25 – 0.3 mm (width 0.75 – 1.1% c)	0.6 – 21.3 %c	Cyclic Cloud	↑ Kinematic energy in the near-wall surface withstanding a pressure rise before the separation

	hydrofoil ($c = 100mm$)							↓Quick surface high-pressure pulsations ↓Cyclic behavior of unsteady cloud cavitation ↓ Turbulent velocity fluctuation transferring high momentum fluid into the vicinity of the wall surface Changing vortex structures and the hydrofoil wake region
Kadivar et al. [181] (2019)	$Cylindrical\ cavitati$ $bubble\ generators$ $on\ CAV2003$ $benchmark\ hydrofo$ ($c = 100mm$)	$6\ m/s$ (6×10^5)	7°	0.8	$0.25 - 0.3\ mm$ ($D = 1.1 - 4\%c$)	6–66%c (1% c)	Cyclic cloud	↓Adverse pressure gradient at the closure region of cavity ↓ Re-entry jet strength ↓Cavitation-induced vibration ↓Near surface high pressure picks Mitigation of cloud cavitation instabilities
Kadivar et al. [182] (2019)	Cylindrical cavitating bubble generators on CAV2003 benchmark hydrofoil (c= 100mm)	($1.4 - 1.5 \times 10^6$)	NA	NA	$1\ mm$ ($D = 1\ mm$)	36% (4%)	Cyclic cloud	↓ large-scale cavitation clouds ↓ pressure pulsations at the wake region Shedding happened only in small-scale cavity

Che et al. [171, 184, 186] (2017-2019)	Delta-shaped counter-rotating VGs on NACA0015 hydrofoil ($c = 100, S = 200\ mm$)	$7\ m/s$ (0.6×10^6)	$6.5 - 8°$	$0.8 - 1.7$	$0.05 - 0.25\ mm$ ($0.5 - 2.5$) ($l = 0.4\ mm$, $\beta = 18°$)	2.5%	Sheet Cavitation	↑ Momentum trans- fer toward the surface ↑ Cavitation length ↓Dominant frequency of cavitation (TCO and PCO condition) ↑Vortex cavitation length by decreasing height of mVGs ↓ Flow disturbance in the span-wise direction Suppression of boundary layer separation Induce inception of vortex cavitation Cavity moving toward leading-edge Vanishing classical fingering structures & Tollmien–Schlichting waves Creating a uniform sheet cavity in the span-wise direction Suppressing R-T and K-H instabilities
Kadivar et al. [178] (2020)	Wedge-type cavitating bubble generators on	$(1.1 \times 10^6 - 1.6 \times 10^6)$	$5, 7, 11°$	$0.66 - 1.3$	NA	NA	Cyclic Cloud	↓ Amplitude of pressure pulsations Hampering a re-entrant jet

	CAV2003 benchmark hydrofoil ($c = 100mm$)							Hindering cloud cavities
Qiu et al. [187] (2020)	Delta-shaped counter-rotating VGs on NACA0015 hydrofoil ($c = 100, S = 200\ mm$)	$10\ m/s$ (1.37×10^6)	6.5, 8	1.35&1.7	$0.25\ mm$ (2.5) ($l = 0.4$, $\beta = 18°$)	2.5%	Attached cavitation	New cavitation structure including vortex cavitation-transition region-attached cavitation Not possible to delay or suppress the attached cavitation in these conditions More stable sheet cavitation More shedding in cloud cavity
Huang et al. [188] (2020)	VGs on Ship propeller	14.37m/s	0– 45	0.2916	$20mm$	NA	Sheet Cavitation	↓Pressure fluctuation ↓Cavitation instability Inducing more uniform wake
Xu et al. [180] (2020)	A cavitator on the lower side of the NACA0012 foil (c=38.1 mm, S=152.4)	NA	1-12	0.1,0.2,.04	5mm	3.125, 6.25, 12.5, 25%c	Supercavitation	Changing the cavitation shape and affect the pressure distribution around the hydrofoil limitation to the effectiveness of the cavitator used for enhancing lift coefficients, since the cavity cannot grow continuously at the

								cavitator to enclose the hydrofoil in the flow.
Chen et al.[191] (2021)	Delta-shaped counter-rotating VGs on Aeronautics 66 hydrofoil at two different position (c=100mm, S=150mm)	1 m/s (1×10^6)	4-12	0.1-5	0.1 mm	0.1%c &0.45% c	Cavitation Inception	Vortex generators located upstream of the laminar separation point promote the earlier inception cavitation and induces the fingerlike vortex cavitation earlier Vortex generators located in the laminar separation zone delays the inception

895

3. Conclusion

This study reviewed different passive flow control techniques with a focus on control cavitation application. The review of passive flow control devices in aerodynamic application showed the potential of passive flow control methods in boundary layer separation, generating stream-wise vortices in the boundary layer, transferring momentum near the wall, delaying and suppression of boundary layer separation, and pressure recovery downstream of vortex generators. The vortex generators showed a better potential for controlling boundary layer separation than other passive flow control methods. Among different types of vortex generators, counter-rotating and co-rotating with $0.2<h/\delta<0.5$ and the distance of 5 to 30h from the upstream of baseline separation showed better effectiveness in controlling and suppressing boundary layer separation.

The review of passive flow control techniques in the hydraulic system shows the effectiveness of this method's different cavitation control types. Different studies in this field have proven the ability of passive flow control methods in suppressing and delaying boundary layer separation and reduction in cavity length and cavitation growth. Many studies observed the generation of stream-wise vortices and reduction in boundary layer span-wise non-uniformities. Besides, transferring high momentum fluid from free stream flow moved to the near-wall low energy region and moving higher kinetic energy flow to the surface's vicinity was another observation in these studies. Declining pressure gradient and intensity of pressure fluctuation at separation point and increasing resistance against pressure rise before boundary layer separation is another result of using passive flow control methods. As re-entrant jets play an important role in cavitation, the effect of passive flow control was weakening the re-entrant jets, their penetration depth, and suppressing the propagation of the pressure wave of collapse. They are also effective in declining the recirculation

zone thickness and consequently the velocity of re-entrant jets. In some experiments, passive flow control methods could delay cavitation inception, while there were some results with earlier cavitation onset.

However, there is no study comparing different types of passive flow control in the same condition in controlling cavitation. In addition to all the effects mentioned above, Vortex generators can eliminate classical "fingering structures" and Tollmien–Schlichting waves and affect partial cavity oscillation, transitional cavity oscillation, and the transition between these two instabilities. They are also effective in declining turbulent velocity fluctuation and decreasing cavitation erosion.

Few studies focused on the Vortex generators in micro-scale [171, 174, 177, 181, 182, 184, 186]. The most recent research in the field of Vortex generators and its effect on the cavitation instabilities was based on the vane-type counter-rotating vortex generator with a minimum height of 0.05mm (0.074 in manufacturing) with $h/\delta = 0.5$ [171, 184, 186]. According to single-phase flow studies of Vortex generators the most optimum h/δ range for Vortex generators is $0.2 < h/\delta < 0.5$. Che et al. [171] stated that because of manufacturing limits they could not manufacture vortex generators with h/δ less than 0.74, and 3D printing could be a solution for manufacturing vortex generators of lower height and thinner thickness and might be relatively easy to be installed in fluid machinery.

According to this review, the potential and effectiveness of passive flow control, and specifically Vortex generators, have been proven. However, there is great potential to optimize designs in terms of geometry, arrangement, and distance to the boundary layer separation. Since the major research in optimizing the design of vortex generators was based on the compressible single phase flow experiments and according to the different nature of compressible and multiphase flows in cavitation phenomenon, the analysis of optimized geometry criteria such as h/δ and l/h and, $\Delta X_{VG}/h$ in hydraulic systems is necessary. Areas for additional investigation include manufacturing

processes including their life-time and durability. Additionally, the specific application area of hydraulic systems, and particular centrifugal pumps, requires greater investigation due to the economic and sustainability gains which might be realized from further optimization of these technologies.

Acknowledgements

This work is funded from the European Union's Horizon 2020 research and innovation programme under grant agreement No. 862100 (NewSkin).

References

1. J.-P. Franc, andJ.-M. Michel, *Fundamentals of Cavitation* (Springer Netherlands, 2005).

2. Q. Wu, B. Huang, G. Wang, S. Cao, andM. Zhu, "Numerical modelling of unsteady cavitation and induced noise around a marine propeller," Ocean Engineering **160**, 143 (2018).

3. D. Valentín, A. Presas, M. Egusquiza, C. Valero, andE. Egusquiza, "Transmission of High Frequency Vibrations in Rotating Systems. Application to Cavitation Detection in Hydraulic Turbines," Applied Sciences **8**, 451 (2018).

4. S. Mouvanal, D. Chatterjee, S. Bakshi, A. Burkhardt, andV. Mohr, "Numerical prediction of potential cavitation erosion in fuel injectors," International Journal of Multiphase Flow **104**, 113 (2018).

5. Y. Hao, andL. Tan, "Symmetrical and unsymmetrical tip clearances on cavitation performance and radial force of a mixed flow pump as turbine at pump mode," Renewable Energy **127**, 368 (2018).

6. O. Reynolds, "The causes of the racing of the engines of screw steamers investigated theoretically and by experiment," Trans. Inst. Naval Arch **14:56-57**, (1873).

7. R. E. A. Arndt, "Cavitation in Fluid Machinery and Hydraulic Structures," Annu. Rev. Fluid Mech. **13**, 273 (1981).

8. A. J. Acosta, "Hydrofoils and Hydrofoil Craft," Annu. Rev. Fluid Mech. **5**, 161 (1973).

9. C. E. Brennen, *Cavitating Flows* (Cambridge University Press, Cambridge, 2013).

10. S. L. Ceccio, andC. E. Brennen, "Observations of the dynamics and acoustics of travelling bubble cavitation," Journal of Fluid Mechanics **233**, 633 (1991).

11. R. W. Kermeen, *Water tunnel tests of NACA 4412 and Walchner profile 7 hydrofoils in noncavitating and cavitating flows* (1956).

12. H. Ganesh, S. A. Mäkiharju, andS. L. Ceccio, "Bubbly shock propagation as a mechanism for sheet-to-cloud transition of partial cavities," Journal of Fluid Mechanics **802**, 37 (2016).

13. M. van Rijsbergen, *A review of sheet cavitation inception mechanisms* (Honolulu, United States, 2016).

14. E. Amromin, *Approximate analysis of hydrofoil material impact on cavitation inception* (Honolulu, United States, 2016).

15. M. Farhat, F. a. Gennoun, andF. o. Avellan, *The Leading Edge Cavitation Dynamics* (2002).

16. E. Ezzatneshan, "Study of surface wettability effect on cavitation inception by implementation of the lattice Boltzmann method," Physics of Fluids **29**, 113304 (2017).

17. T. F. Groß, andP. F. Pelz, "Diffusion-driven nucleation from surface nuclei in hydrodynamic cavitation," Journal of Fluid Mechanics **830**, 138 (2017).

18. V. H. Arakeri, "Viscous effects on the position of cavitation separation from smooth bodies," Journal of Fluid Mechanics **68**, 779 (1975).

19. A. T. Leger, andS. L. Ceccio, "Examination of the flow near the leading edge of attached cavitation. Part 1. Detachment of two-dimensional and axisymmetric cavities," Journal of Fluid Mechanics **376**, 61 (1998).

20. V. H. Arakeri, andA. J. Acosta, "Viscous Effects in the Inception of Cavitation on Axisymmetric Bodies," Journal of Fluids Engineering **95**, 519 (1973).

21. J. P. Franc, andJ. M. Michel, "Attached cavitation and the boundary layer: experimental investigation and numerical treatment," Journal of Fluid Mechanics **154**, 63 (1985).

22. S. Scott Collis, R. D. Joslin, A. Seifert, andV. Theofilis, "Issues in active flow control: theory, control, simulation, and experiment," Progress in Aerospace Sciences **40**, 237 (2004).

23. M. Gad-el-Hak, *Flow Control: Passive, Active, and Reactive Flow Management* (Cambridge University Press, Cambridge, 2000).

24. T. Moghaddam, andN. B. Neishabouri, "On the Active and Passive Flow Separation Control Techniques over Airfoils," IOP Conference Series: Materials Science and Engineering **248**, 012009 (2017).

25. M. Genç, K. Koca, H. Demir, andH. Açıkel, *Traditional and New Types of Passive Flow Control Techniques to Pave the Way for High Maneuverability and Low Structural Weight for UAVs and MAVs* (2020).

26. J. C. Lin, "Review of research on low-profile vortex generators to control boundary-layer separation," Progress in Aerospace Sciences **38**, 389 (2002).

27. L. Howarth, andG. I. Taylor, "Concerning the effect of compressibility on lam inar boundary layers and their separation," Proceedings of the Royal Society of London. Series A. Mathematical and Physical Sciences **194**, 16 (1948).

28. K. Stewartson, "Correlated Incompressible and Compressible Boundary Layers," Proceedings of the Royal Society of London. Series A, Mathematical and Physical Sciences **200**, 84 (1949).

29. O. Lögdberg, "Vortex generators and turbulent boundary layer separation control," Licentiate thesis, monograph KTH, 2006.

30. B. Munson, D. Young, andT. Okiishi, "Fundamentals of Fluid Mechanics," Fundamentals of fluid mechanics (2002).

31. NASA, *Drag of a Sphere* (NASA, Glenn research center).

32. M. S. Genç, Ü. Kaynak, andG. D. Lock, "Flow over an aerofoil without and with a leading-edge slat at a transitional Reynolds number," Proceedings of the Institution of Mechanical Engineers, Part G: Journal of Aerospace Engineering **223**, 217 (2009).

33. L. Traub, andM. Kaula, "Effect of Leading-Edge Slats at Low Reynolds Numbers," Aerospace **3**, 39 (2016).

34. G. Pechlivanoglou, "Passive and active flow control solutions for wind turbine blades," Doctoral Thesis Technische Universität Berlin, 2013.

35. Z. Wang, andM. Zhuang, "Leading-edge serrations for performance improvement on a vertical-axis wind turbine at low tip-speed-ratios," Applied Energy **208**, 1184 (2017).

36. S. Beyhaghi, andR. S. Amano, "A parametric study on leading-edge slots used on wind turbine airfoils at various angles of attack," Journal of Wind Engineering and Industrial Aerodynamics **175**, 43 (2018).

37. G. Godard, andM. Stanislas, "Control of a decelerating boundary layer. Part 1: Optimization of passive vortex generators," Aerospace Science and Technology **10**, 181 (2006).

38. A. S. Shehata, Q. Xiao, K. M. Saqr, A. Naguib, andD. Alexander, "Passive flow control for aerodynamic performance enhancement of airfoil with its application in Wells turbine – Under oscillating flow condition," Ocean Engineering **136**, 31 (2017).

39. W. W. R. T. a. D. Huebsch, "Numerical investigation on the interaction between surface roughness and viscous flows " Iowa State University, 2000.

40. M. Serdar GenÇ, K. Koca, andH. H. AÇIkel, "Investigation of pre-stall flow control on wind turbine blade airfoil using roughness element," Energy **176**, 320 (2019).

41. K. Koca, M. S. Genç, H. H. Açıkel, M. Çağdaş, andT. M. Bodur, "Identification of flow phenomena over NACA 4412 wind turbine airfoil at low Reynolds numbers and role of laminar separation bubble on flow evolution," Energy **144**, 750 (2018).

42. M. S. Genç, K. Koca, H. H. Açıkel, G. Özkan, M. S. Kırış, andR. Yıldız, "Flow characteristics over NACA4412 airfoil at low Reynolds number," EPJ Web of Conferences **114**, (2016).

43. M. Gad-el-Hak, "Modern Developments in Flow Control," Applied Mechanics Reviews **49**, 365 (1996).

44. A. M. Kuethe, "Effect of streamwise vortices on wake properties associated with sound generation," Journal of Aircraft **9**, 715 (1972).

45. D. Rao, andT. Kariya, *Boundary-layer submerged vortex generators for separation control - An exploratory study* (American Institute of Aeronautics and Astronautics, 1988).

46. J. C. Lin, F. G. Howard, andG. V. Selby, "Small submerged vortex generators for turbulent flow separation control," Journal of Spacecraft and Rockets **27**, 503 (1990).

47. J. Lin, F. Howard, andG. Selby, *Exploratory study of vortex-generating devices for turbulent flow separation control* (American Institute of Aeronautics and Astronautics, 1991).

48. M. Kerho, S. Hutcherson, R. F. Blackwelder, andR. H. Liebeck, "Vortex generators used to control laminar separation bubbles," Journal of Aircraft **30**, 315 (1993).

49. J. Lin, F. Howard, D. Bushnell, andG. Selby, *Investigation of several passive and active methods for turbulent flow separation control* (American Institute of Aeronautics and Astronautics, 1990).

50. J. Lin, *Control of turbulent boundary-layer separation using micro-vortex generators* (American Institute of Aeronautics and Astronautics, 1999).

51. S. Gorton, L. Jenkins, andS. Anders, *Flow control device evaluation for an internal flow with an adverse pressure gradient* (American Institute of Aeronautics and Astronautics, 2002).

52. J. C. Lin, S. K. Robinson, R. J. McGhee, andW. O. Valarezo, "Separation control on high-lift airfoils via micro-vortex generators," Journal of Aircraft **31**, 1317 (1994).

53. T. Tai, *Effect of micro-vortex generators on V-22 aircraft forward-flight aerodynamics* (American Institute of Aeronautics and Astronautics, 2002).

54. P. Ashill, J. Fulker, andK. Hackett, *Studies of flows induced by Sub Boundary Layer Vortex Generators (SBVGs)* (American Institute of Aeronautics and Astronautics, 2002).

55. P. Ashill, J. Fulker, andK. Hackett, *Research at DERA on sub boundary layer vortex generators (SBVGs)* (American Institute of Aeronautics and Astronautics, 2001).

56. J. W. Hamstra, D. N. Miller, P. P. Truax, B. A. Anderson, andB. J. Wendt, "Active inlet flow control technology demonstration," The Aeronautical Journal (1968) **104**, 473 (2000).

57. C. Yao, J. Lin, andB. Allen, *Flowfield Measurement of Device-Induced Embedded Streamwise Vortex on a Flat Plate* (American Institute of Aeronautics and Astronautics, 2002).

58. B. Allan, C.-S. Yao, andJ. Lin, *Numerical Simulations of Vortex Generator Vanes and Jets on a Flat Plate* (American Institute of Aeronautics and Astronautics, 2002).

59. H. Holden, andH. Babinsky, *Vortex Generators near Shock/ Boundary Layer Interactions* (American Institute of Aeronautics and Astronautics, 2004).

60. H. Babinsky, Y. Li, andC. W. P. Ford, "Microramp Control of Supersonic Oblique Shock-Wave/Boundary-Layer Interactions," AIAA Journal **47**, 668 (2009).

61. S. Ghosh, J.-I. Choi, andJ. R. Edwards, "Numerical Simulations of Effects of Micro Vortex Generators Using Immersed-Boundary Methods," AIAA Journal **48**, 92 (2010).

62. X. Dong, Y. Chen, G. Dong, andY. Liu, "Study on wake structure characteristics of a slotted micro-ramp with large-eddy simulation," Fluid Dynamics Research **49**, 035507 (2017).

63. Z. Sun, F. Schrijer, F. Scarano, andB. Oudheusden, "Decay of the supersonic turbulent wakes from micro-ramps," Physics of Fluids **26**, 025115 (2014).

64. Q. Li, andC. Liu, *LES for Supersonic Ramp Control Flow Using MVG at M=2.5 and Re?=1440* (American Institute of Aeronautics and Astronautics, 2010).

65. Z. Sun, F. F. J. Schrijer, F. Scarano, andB. W. van Oudheusden, "The three-dimensional flow organization past a micro-ramp in a supersonic boundary layer," Physics of Fluids **24**, 055105 (2012).

66. DongSun, JianqiangChen, ChenLi, PengxinLiu, QilongGuo, andXianxuYuan, "On the wake structure of a micro-ramp vortex generator in hypersonic flow," Physics of Fluids **32**, 126111 (2020).

67. D. Sun, Q. Guo, C. Li, andP. Liu, "Direct numerical simulation of effects of a micro-ramp on a hypersonic shock wave/boundary layer interaction," Physics of Fluids **31**, 126101 (2019).

68. M. Z. Akhter, andF. K. Omar, "Review of Flow-Control Devices for Wind-Turbine Performance Enhancement," Energies **14**, (2021).

69. J. Franc, *Physics and Control of Cavitation Jean-Pierre FRANC University of Grenoble LEGI@ BP 53 38041 Grenoble Cedex 9 FRANCE* (2008).

70. Q. Chen, Y. Liu, Q. Wu, Y. Wang, T. Liu, andG. Wang, "Global cavitation patterns and corresponding hydrodynamics of the hydrofoil with leading edge roughness," Acta Mechanica Sinica **36**, 1202 (2020).

71. O. De La Torre, X. Escaler, E. Egusquiza, andM. Farhat, "Experimental investigation of added mass effects on a hydrofoil under cavitation conditions," Journal of Fluids and Structures **39**, 173 (2013).

72. M. Kadivar, D. Tormey, andG. McGranaghan, "A review on turbulent flow over rough surfaces: Fundamentals and theories," International Journal of Thermofluids **10**, 100077 (2021).

73. H. L. Dryden, "Review of Published Data on the Effect of Roughness on Transition from Laminar to Turbulent Flow," Journal of the Aeronautical Sciences **20**, 477 (1953).

74. M. F. Kerho, andM. B. Bragg, "Airfoil Boundary-Layer Development and Transition with Large Leading-Edge Roughness," AIAA Journal **35**, 75 (1997).

75. B. Stutz, "Influence of Roughness on the Two-Phase Flow Structure of Sheet Cavitation," Journal of Fluids Engineering **125**, 652 (2003).

76. O. Coutier-Delgosha, J.-F. Devillers, M. Leriche, andT. Pichon, "Effect of Wall Roughness on the Dynamics of Unsteady Cavitation," Journal of Fluids Engineering **127**, 726 (2005).

77. P. Ausoni, M. Farhat, andF. Avellan, "Hydrofoil Roughness Effects on von Kármán Vortex Shedding," (2007).

78. P. Ausoni, A. Zobeiri, F. Avellan, andM. Farhat, "The Effects of a Tripped Turbulent Boundary Layer on Vortex Shedding from a Blunt Trailing Edge Hydrofoil," Journal of Fluids Engineering **134**, (2012).

79. P. L. Delafin, F. Deniset, andJ. A. Astolfi, "Effect of the laminar separation bubble induced transition on the hydrodynamic performance of a hydrofoil," European Journal of Mechanics - B/Fluids **46**, 190 (2014).

80. M. Petkovšek, Ho, ccaron, M. evar, Gregor, ccaron, ccaron, andP. , *Cavitation Dynamics on Laser-Textured Surfaces* (ASME Press, 2018).

81. A. M. Emelyanenko, F. M. Shagieva, A. G. Domantovsky, andL. B. Boinovich, "Nanosecond laser micro- and nanotexturing for the design of a superhydrophobic coating robust against long-term contact with water, cavitation, and abrasion," Applied Surface Science **332**, 513 (2015).

82. R. Tao, R. Xiao, andM. Farhat, "Effect of leading edge roughness on cavitation inception and development on thin hydrofoil," Paiguan Jixie Gongcheng Xuebao/Journal of Drainage and Irrigation Machinery Engineering **35**, 921 (2017).

83. S. A. Churkin, K. S. Pervunin, A. Y. Kravtsova, D. M. Markovich, andK. Hanjalić, "Cavitation on NACA0015 hydrofoils with different wall roughness: high-speed visualization of the surface texture effects," Journal of Visualization **19**, 587 (2016).

84. K. Onishi, K. Matsuda, andK. Miyagawa, *Influence of hydrophilic and hydrophobic coating on hydrofoil performance* (2017).

85. J. Hao, M. Zhang, andX. Huang, "The influence of surface roughness on cloud cavitation flow around hydrofoils," Acta Mechanica Sinica **34**, 10 (2018).

86. A. Asnaghi, U. Svennberg, R. Gustafsson, andR. E. Bensow, "Investigations of tip vortex mitigation by using roughness," Physics of Fluids **32**, 065111 (2020).

87. U. Svennberg, A. Asnaghi, R. Gustafsson, andR. Bensow, *Experimental Analysis of Tip Vortex Cavitation Mitigation By Controlled Surface Roughness* (2020).

88. X. Lv, W. T. Wu, J. Lv, K. Mao, L. Gao, andY. Li, "Study on the law of pseudo-cavitation on superhydrophobic surface in turbulent flow field of backward-facing step," Fluids **6**, (2021).

89. H. Kim, andC. Kim, "A physics-based cavitation model ranging from inertial to thermal regimes," International Journal of Heat and Mass Transfer **181**, (2021).

90. M. Adama Maiga, O. Coutier-Delgosha, andD. Buisine, "A new cavitation model based on bubble-bubble interactions," Physics of Fluids **30**, (2018).

91. O. Ivashnev, M. Ivashneva, andN. Smirnov, "Rarefaction waves in nonequilibrium-boiling fluid flows," Fluid Dynamics - FLUID DYN **35**, 485 (2000).

92. A. A. Aganin, andT. F. Khalitova, "Calculation of Small Deformations of a Radially Convergent Shock Wave Inside a Cavitation Bubble," Lobachevskii Journal of Mathematics **42**, 1954 (2021).

93. M. Zhang, Q. Chang, X. Ma, G. Wang, andB. Huang, "Physical investigation of the counterjet dynamics during the bubble rebound," Ultrasonics Sonochemistry **58**, (2019).

94. A. A. Aganin, A. I. Davletshin, andT. F. Khalitova, "Expansion and Collapse of Bubbles in the Central Region of a Streamer," Lobachevskii Journal of Mathematics **42**, 15 (2021).

95. O. Ivashnyov , M. Ivashneva, andN. Smirnov, "Slow waves of boiling under hot water depressurization," Journal of Fluid Mechanics **413**, 149 (2000).

96. X. Tang, X. Duan, H. Gao, X. Li, andX. Shi, "CFD investigations of transient cavitation flows in pipeline based on weakly-compressible model," Water (Switzerland) **12**, (2020).

97. V. K. Kedrinskiy, andE. S. Zhuravleva, *Formation of a cavitation zone behind a rarefaction wave front in a shock-loaded thin layer of a multiphase liquid* (2019).

98. A. Fraters, M. Van Den Berg, Y. De Loore, H. Reinten, H. Wijshoff, D. Lohse, M. Versluis, andT. Segers, "Inkjet Nozzle Failure by Heterogeneous Nucleation: Bubble Entrainment, Cavitation, and Diffusive Growth," Physical Review Applied **12**, (2019).

99. E. S. Zhuravleva, andV. K. Kedrinskii, "Focusing of the Rarefaction Wave in a Thin Cavitating Fluid Layer with a Free Boundary," Journal of Applied Mechanics and Technical Physics **59**, 1004 (2018).

100. N. Kyriazis, P. Koukouvinis, andM. Gavaises, "Modelling cavitation during drop impact on solid surfaces," Advances in Colloid and Interface Science **260**, 46 (2018).

101. O. E. Ivashnyov, andN. N. Smirnov, "Thermal growth of a vapor bubble moving in superheated liquid," Physics of Fluids **16**, 809 (2004).

102. R. I. Nigmatulin, J. R. T. Lahey, R. P. Taleyarkhan, C. D. West, andR. C. Block, "On thermonuclear processes in cavitation bubbles," Physics-Uspekhi **57**, 877 (2014).

103. Y. Liu, andY. Peng, "Study on the collapse process of cavitation bubbles including heat transfer by lattice boltzmann method," Journal of Marine Science and Engineering **9**, 1 (2021).

104. M. Gallo, F. Magaletti, D. Cocco, andC. M. Casciola, "Nucleation and growth dynamics of vapour bubbles," Journal of Fluid Mechanics **883**, (2020).

105. J. Zhu, S. Wang, andX. Zhang, "Influences of thermal effects on cavitation dynamics in liquid nitrogen through venturi tube," Physics of Fluids **32**, (2020).

106. D. Papoulias, andM. Gavaises, *Modelling of single bubble-dynamics and thermal effects* (2015).

107. M. T. Warnez, andE. Johnsen, "Numerical modeling of bubble dynamics in viscoelastic media with relaxation," Physics of Fluids **27**, (2015).

108. A. A. Aganin, O. R. Ganiev, A. I. Davletshin, andL. E. Ukrainskii, "Evaluation of Thermal and Acoustic Energy during Collapse of Cavitation Bubbles," Journal of Machinery Manufacture and Reliability **49**, 367 (2020).

109. A. A. Aganin, O. R. Ganiev, A. I. Davletshin, andL. E. Ukrainskyi, "Liquid Heating During the Collapse of a Single Cavitation Bubble," Journal of Machinery Manufacture and Reliability **49**, 24 (2020).

110. R. I. Nigmatulin, A. A. Aganin, andD. Y. Toporkov, "Possibility of Cavitation Bubble Supercompression in Tetradecane," Doklady Physics **63**, 348 (2018).

111. A. A. Aganin, andT. F. Khalitova, *Small non-sphericity of a convergent shock wave arising in a cavitation bubble in acetone during its collapse* (2020).

112. A. A. Aganin, M. A. Il'gamov, R. I. Nigmatulin, andD. Y. Toporkov, "Evolution of distortions of the spherical shape of a cavitation bubble in acoustic supercompression," Fluid Dynamics **45**, 50 (2010).

113. S. Park, andG. Son, "Numerical study of the effect of liquid compressibility on acoustic droplet vaporization," Ultrasonics Sonochemistry **79**, (2021).

114. Y. H. Chen, J. M. Zhan, andY. T. Li, "Numerical simulation of cavitation-bubble expansion and collapse inside a bottle subjected to impact on its topside," Engineering Applications of Computational Fluid Mechanics **15**, 1440 (2021).

115. F. Denner, "The Gilmore-NASG model to predict single-bubble cavitation in compressible liquids," Ultrasonics Sonochemistry **70**, (2021).

116. R. F. Ganiev, A. A. Aganin, O. R. Ganiev, G. N. Granova, A. I. Davletshin, L. E. Ukrainskii, andI. G. Ustenko, "Compression of cavitation bubble in viscous liquid," Journal of Machinery Manufacture and Reliability **46**, (2017).

117. M. Sivčák, andT. Hruš, *Influence of bubbles in the shock liquid at its compressibility* (2017).

118. T. Trummler, S. J. Schmidt, andN. A. Adams, "Numerical investigation of non-condensable gas effect on vapor bubble collapse," Physics of Fluids **33**, (2021).

119. U. Iben, A. Makhnov, andA. Schmidt, *Numerical Investigation of Cavitating Flows with Liquid Degassing* (2018).

120. J. Lee, *Importance of sonication and solution conditions on the acoustic cavitation activity #5* (2016).

121. E. Kadivar, O. e. Moctar, R. Skoda, andU. Löschner, "Experimental study of the control of cavitation-induced erosion created by collapse of single bubbles using a micro structured riblet," Wear **486-487**, 204087 (2021).

122. S. R. Gonzalez-Avila, D. M. Nguyen, S. Arunachalam, E. M. Domingues, H. Mishra, andC.-D. Ohl, "Mitigating cavitation erosion using biomimetic gas-entrapping microtextured surfaces (GEMS)," Science Advances **6**, eaax6192 (2020).

123. Y. T. Shen, andR. Eppler, "Wing Sections for Hydrofoils—Part 2: Nonsymmetrical Profiles," Journal of Ship Research **25**, 191 (1981).

124. Y. T. Shen, "Wing Sections for Hydrofoils—Part 3: Experimental Verifications," Journal of Ship Research **29**, 39 (1985).

125. S. Kyparissis, andD. Margaris, "Experimental investigation of cavitation in a centrifugal pump with double-arc synthetic blade design method," International Review of Mechanical Engineering **5**, 884 (2011).

126. S. D. Kyparissis, andD. P. Margaris, "Experimental Investigation and Passive Flow Control of a Cavitating Centrifugal Pump," International Journal of Rotating Machinery **2012**, 248082 (2012).

127. W. Shi, M. Atlar, R. Rosli, B. Aktas, andR. Norman, "Cavitation observations and noise measurements of horizontal axis tidal turbines with biomimetic blade leading-edge designs," Ocean Engineering **121**, 143 (2016).

128. C. B. Senel, H. Maral, L. A. Kavurmacioglu, andC. Camci, "An aerothermal study of the influence of squealer width and height near a HP turbine blade," International Journal of Heat and Mass Transfer **120**, 18 (2018).

129. C. Camci, D. Dey, andL. Kavurmacioglu, "Aerodynamics of Tip Leakage Flows Near Partial Squealer Rims in an Axial Flow Turbine Stage," Journal of Turbomachinery **127**, 14 (2005).

130. J. H. Cheon, andS. W. Lee, "Tip leakage aerodynamics over the cavity squealer tip equipped with full coverage winglets in a turbine cascade," International Journal of Heat and Fluid Flow **56**, 60 (2015).

131. M. Lei, andZ. Junwei, *Effects of Blade Tip Foil Thickening on Tip Vortexes in Ducted Propeller* (Atlantis Press, 2015).

132. Q. Guo, L. Zhou, andZ. Wang, "Numerical evaluation of the clearance geometries effect on the flow field and performance of a hydrofoil," Renewable Energy **99**, 390 (2016).

133. S. Q. Wu, W. D. Shi, D. S. Zhang, J. Yao, andC. Cheng, "Influence of blade tip rounding on tip leakage vortex cavitation of axial flow pump," IOP Conference Series: Materials Science and Engineering **52**, 062011 (2013).

134. Y. Liu, andL. Tan, "Method of C groove on vortex suppression and energy performance improvement for a NACA0009 hydrofoil with tip clearance in tidal energy," Energy **155**, 448 (2018).

135. D. Kang, Y. Arimoto, K. Yonezawa, H. Horiguchi, Y. Kawata, C. Hah, andY. Tsujimoto, "Suppression of Cavitation Instabilities in an Inducer by Circumferential Groove and Explanation of Higher Frequency Components," International Journal of Fluid Machinery and Systems **3**, 137 (2010).

136. M. Dreyer, "Mind The Gap: Tip Leakage Vortex Dynamics and Cavitation in Axial Turbines," 2015.

137. H.-y. Cheng, B. Ji, X.-p. Long, andM. Farhat, "A review of cavitation in tip-leakage flow and its control," Journal of Hydrodynamics **33**, (2021).

138. D. Custodio, C. Henoch, andH. Johari, "Cavitation on hydrofoils with leading edge protuberances," Ocean Engineering **162**, 196 (2018).

139. W. G. Zhao, andG. Wang, "Research on passive control of cloud cavitation based on a bionic fin-fin structure," Engineering Computations **37**, 863 (2019).

140. R. Kant, andA. Bhattacharyya, "A bio-inspired twin-protuberance hydrofoil design," Ocean Engineering **218**, 108209 (2020).

141. D. Li, Q. Yang, W. Yang, H. Chang, andH. Wang, "Bionic leading-edge protuberances and hydrofoil cavitation," Physics of Fluids **33**, 093317 (2021).

142. J. Li, C. Liu, andX. Li, "Effects of Wavy Leading-Edge Protuberance on Hydrofoil Performance and Its Flow Mechanism," Journal of Marine Science and Engineering **9**, (2021).

143. R. García-Mayoral, andJ. Jiménez, "Drag reduction by riblets," Philosophical Transactions of the Royal Society A: Mathematical, Physical and Engineering Sciences **369**, 1412 (2011).

144. W. Li, W. Jessen, D. Roggenkamp, M. Klaas, W. Silex, M. Schiek, andW. Schröder, "Turbulent drag reduction by spanwise traveling ribbed surface waves," European Journal of Mechanics - B/Fluids **53**, 101 (2015).

145. F. E. Fish, andG. V. Lauder, "PASSIVE AND ACTIVE FLOW CONTROL BY SWIMMING FISHES AND MAMMALS," Annu. Rev. Fluid Mech. **38**, 193 (2005).

146. Y. Li, H. Chen, J. Wang, andD. Chen, "Effect of Grooves on Cavitation Around the Body of Revolution," Journal of Fluids Engineering **132**, (2009).

147. A. Danlos, F. Ravelet, O. Coutier-Delgosha, andF. Bakir, "Cavitation regime detection through Proper Orthogonal Decomposition: Dynamics analysis of the sheet cavity on a grooved convergent–divergent nozzle," International Journal of Heat and Fluid Flow **47**, 9 (2014).

148. A. Danlos, J.-E. Méhal, F. Ravelet, O. Coutier-Delgosha, andF. Bakir, "Study of the Cavitating Instability on a Grooved Venturi Profile," Journal of Fluids Engineering **136**, (2014).

149. Y. Liu, andL. Tan, "Method of C groove on vortex suppression and energy performance improvement for a NACA0009 hydrofoil with tip clearance in tidal energy," Energy **155**, 448 (2018).

150. H. Cheng, X. Long, B. Ji, X. Peng, andM. Farhat, "Suppressing tip-leakage vortex cavitation by overhanging grooves," Experiments in Fluids **61**, 159 (2020).

151. H. Kato, H. Yamaguchi, S. Okada, K. Kikuchi, andM. Miyanaga, "Suppression of Sheet Cavitation Inception by Water Discharge Through Slit," Journal of Fluids Engineering **109**, 70 (1987).

152. R. E. A. Arndt, C. R. Ellis, andS. Paul, "Preliminary Investigation of the Use of Air Injection to Mitigate Cavitation Erosion," Journal of Fluids Engineering **117**, 498 (1995).

153. K. N. O. David Japikse, Daniel O. Baun STABILITY ENHANCEMENT OF COMPRESSORS AND TURBOPUMPS BY PASSIVE FLOW CONTROL Document No. Number, 2006.

154. B. Zhu, H. Chen, andQ. Wei, "Numerical and Experimental Investigation of Cavitating Characteristics in Centrifugal Pump with Gap Impeller," International Journal of Turbo and Jet Engines **31**, 187 (2014).

155. Z. Bing, andC. Hongxun, "Analysis of the Staggered and Fixed Cavitation Phenomenon Observed in Centrifugal Pumps Employing a Gap Drainage Impeller," Journal of Fluids Engineering **139**, (2016).

156. Y. Kamikura, H. Kobayashi, S. Kawasaki, andY. Iga, "Three dimensional numerical analysis of inducer about suppression of cavitation instabilities by asymmetric slits on blades," IOP Conference Series: Earth and Environmental Science **240**, 032044 (2019).

157. W. Wang, Q. Yi, S. Lu, andX. Wang, *Exploration and Research of the Impact of Hydrofoil Surface Water Injection on Cavitation Suppression* (2017).

158. Y. Kawanami, H. Kato, H. Yamaguchi, M. Tanimura, andY. Tagaya, "Mechanism and Control of Cloud Cavitation," Journal of Fluids Engineering **119**, 788 (1997).

159. T. Pham, F. Larrarte, andD. Fruman, "Investigation of Unsteady Sheet Cavitation and Cloud Cavitation Mechanisms," Journal of Fluids Engineering-transactions of The Asme - J FLUID ENG **121**, (1999).

160. K. Sato, M. Tanada, S. Monden, andY. Tsujimoto, "Observations of Oscillating Cavitation on a Flat Plate Hydrofoil," JSME International Journal Series B Fluids and Thermal Engineering **45**, 646 (2002).

161. W.-g. Zhao, L.-x. Zhang, X.-m. Shao, andJ. Deng, "Numerical study on the control mechanism of cloud cavitation by obstacles," Journal of Hydrodynamics, Ser. B **22**, 792 (2010).

162. H. Ganesh, S. Mäkiharju, andS. Ceccio, "Interaction of a Compressible Bubbly Flow With an Obstacle Placed Within a Shedding Partial Cavity," Journal of Physics: Conference Series **656**, 012151 (2015).

163. S. Watanabe, N. Enomoto, K. Ishizaka, A. Furukawa, andJ.-H. Kim, "Suppression of Cavitation Surge of a Helical Inducer Occurring in Partial Flow Conditions," Turbomachinery **32**, 94 (2004).

164. J.-H. Kim, K. Ishzaka, S. Watanabe, andA. Furukawa, "Cavitation Surge Suppression of Pump Inducer with Axi-asymmetrical Inlet Plate," International Journal of Fluid Machinery and Systems **3**, 50 (2010).

165. J. Huang, C. Yu, Y. Wang, C. Xu, andC. Huang, "Passive control of cavitating flow around an axisymmetric projectile by using a trip bar," Theoretical and Applied Mechanics Letters **7**, 181 (2017).

166. E. Kadivar, E. Kadivar, K. Javadi, andS. M. Javadpour, "The investigation of natural super-cavitation flow behind three-dimensional cavitators: Full cavitation model," Applied Mathematical Modelling **45**, 165 (2017).

167. B. Che, L. Cao, N. Chu, D. Likhachev, andD. Wu, "Effect of obstacle position on attached cavitation control through response surface methodology," Journal of Mechanical Science and Technology **33**, 4265 (2019).

168. L. Zhang, M. Chen, andX. Shao, "Inhibition of cloud cavitation on a flat hydrofoil through the placement of an obstacle," Ocean Engineering **155**, 1 (2018).

169. G. Zhao, L. Cao, B. Che, R. Wu, S. Yang, andD. Wu, "Towards the control of blade cavitation in a waterjet pump with inlet guide vanes: Passive control by obstacles," Ocean Engineering **231**, 108820 (2021).

170. Z. Lin, J. Tao, D. Yin, andZ. Zhu, "Numerical study on cavitation over flat hydrofoils with arc obstacles," Physics of Fluids **33**, 085101 (2021).

171. B. Che, N. Chu, S. J. Schmidt, L. Cao, D. Likhachev, andD. Wu, "Control effect of micro vortex generators on leading edge of attached cavitation," Physics of Fluids **31**, 044102 (2019).

172. H. An, "On the use of vortex generators to control cavitation in a backward facing step flow," Ph.D. Purdue University, 2007.

173. Y. Liang-mei, "Application of the Vortex Generator to Control the PHV Cavitation," Journal of Ship Mechanics (2009).

174. K. Javadi, M. M. Dorostkar, andA. Katal, "Cavitation passive control on immersed bodies," Journal of Marine Science and Application **16**, 33 (2017).

175. A. Amini, M. Reclari, T. Sano, M. Iino, andM. Farhat, "Suppressing tip vortex cavitation by winglets," Experiments in Fluids **60**, 159 (2019).

176. V. C. Andichamy, G. T. Khokhar, andC. Camci, *An Experimental Study of Using Vortex Generators As Tip Leakage Flow Interrupters in an Axial Flow Turbine Stage* (2018).

177. E. Kadivar, O. e. Moctar, andK. Javadi, "Investigation of the effect of cavitation passive control on the dynamics of unsteady cloud cavitation," Applied Mathematical Modelling **64**, 333 (2018).

178. E. Kadivar, M. V. Timoshevskiy, M. Y. Nichik, O. el Moctar, T. E. Schellin, andK. S. Pervunin, "Control of unsteady partial cavitation and cloud cavitation in marine engineering and hydraulic systems," Physics of Fluids **32**, 052108 (2020).

179. E. Kadivar, M. V. Timoshevskiy, K. S. Pervunin, andO. e. Moctar, "Experimental and numerical study of the cavitation surge passive control around a semi-circular leading-edge flat plate," Journal of Marine Science and Technology **25**, 1010 (2020).

180. C. Xu, andB. C. Khoo, "Dynamics of the supercavitating hydrofoil with cavitator in steady flow field," Physics of Fluids **32**, 123307 (2020).

181. E. Kadivar, O. e. Moctar, andK. Javadi, "Stabilization of cloud cavitation instabilities using Cylindrical Cavitating-bubble Generators (CCGs)," International Journal of Multiphase Flow **115**, 108 (2019).

182. E. Kadivar, M. Timoshevskiy, K. Pervunin, andO. e. Moctar, "Experimental investigation of the passive control of unsteady cloud cavitation using miniature vortex generators (MVGs)," IOP Conference Series: Earth and Environmental Science **405**, 012002 (2019).

183. E. Kadivar, M. V. Timoshevskiy, K. S. Pervunin, andO. e. Moctar, "Cavitation control using Cylindrical Cavitating-bubble Generators (CCGs): Experiments on a benchmark CAV2003 hydrofoil," International Journal of Multiphase Flow **125**, 103186 (2020).

184. B. Che, andD. Wu, *Study on Vortex Generators for Control of Attached Cavitation* (2017).

185. P. K. Kundu, I. M. Cohen, andD. R. Dowling, *Chapter 11 - Instability* (Academic Press, Boston, 2016).

186. B. Che, N. Chu, L. Cao, S. J. Schmidt, D. Likhachev, andD. Wu, "Control effect of micro vortex generators on attached cavitation instability," Physics of Fluids **31**, (2019).

187. N. Qiu, W. Zhou, B. Che, D. Wu, L. Wang, andH. Zhu, "Effects of microvortex generators on cavitation erosion by changing periodic shedding into new structures," Physics of Fluids **32**, (2020).

188. H.-b. Huang, Y. Long, andB. Ji, "Experimental investigation of vortex generator influences on propeller cavitation and hull pressure fluctuations," Journal of Hydrodynamics **32**, 82 (2020).

189. L. Li, B. Zhou, H. Huang, andH. Sun, "Vortex generator design and numerical investigation for wake non-uniformity and cavitation fluctuation pressure reduction," Ocean Engineering **229**, 108965 (2021).

190. O. Teplov, andV. Lomakin, "Improving the performance of a centrifugal vane pump by installing vortex generators on the suction surfaces of blades," IOP Conference Series: Materials Science and Engineering **779**, 012012 (2020).

191. J. Chen, C. Hu, M. Zhang, B. Huang, andH. Zhang, "The influence of micro vortex generator on inception cavitation," Physics of Fluids **33**, 103312 (2021).